Response of ocean ecosystems to climate warming

J. L. Sarmiento,[1] R. Slater,[1] R. Barber,[2] L. Bopp,[3] S. C. Doney,[4] A. C. Hirst,[5] J. Kleypas,[6] R. Matear,[7] U. Mikolajewicz,[8] P. Monfray,[3] V. Soldatov,[9] S. A. Spall,[10] and R. Stouffer[11]

Received 1 August 2003; revised 2 April 2004; accepted 11 May 2004; published 14 July 2004.

[1] We examine six different coupled climate model simulations to determine the ocean biological response to climate warming between the beginning of the industrial revolution and 2050. We use vertical velocity, maximum winter mixed layer depth, and sea ice cover to define six biomes. Climate warming leads to a contraction of the highly productive marginal sea ice biome by 42% in the Northern Hemisphere and 17% in the Southern Hemisphere, and leads to an expansion of the low productivity permanently stratified subtropical gyre biome by 4.0% in the Northern Hemisphere and 9.4% in the Southern Hemisphere. In between these, the subpolar gyre biome expands by 16% in the Northern Hemisphere and 7% in the Southern Hemisphere, and the seasonally stratified subtropical gyre contracts by 11% in both hemispheres. The low-latitude (mostly coastal) upwelling biome area changes only modestly. Vertical stratification increases, which would be expected to decrease nutrient supply everywhere, but increase the growing season length in high latitudes. We use satellite ocean color and climatological observations to develop an empirical model for predicting chlorophyll from the physical properties of the global warming simulations. Four features stand out in the response to global warming: (1) a drop in chlorophyll in the North Pacific due primarily to retreat of the marginal sea ice biome, (2) a tendency toward an increase in chlorophyll in the North Atlantic due to a complex combination of factors, (3) an increase in chlorophyll in the Southern Ocean due primarily to the retreat of and changes at the northern boundary of the marginal sea ice zone, and (4) a tendency toward a decrease in chlorophyll adjacent to the Antarctic continent due primarily to freshening within the marginal sea ice zone. We use three different primary production algorithms to estimate the response of primary production to climate warming based on our estimated chlorophyll concentrations. The three algorithms give a global increase in primary production of 0.7% at the low end to 8.1% at the high end, with very large regional differences. The main cause of both the response to warming and the variation between algorithms is the temperature sensitivity of the primary production algorithms. We also show results for the period between the industrial revolution and 2050 and 2090. *INDEX TERMS:* 1615 Global Change: Biogeochemical processes (4805); 1635 Global Change: Oceans (4203); 4815 Oceanography: Biological and Chemical: Ecosystems, structure and dynamics; *KEYWORDS:* climate warming, ocean biogeochemistry

Citation: Sarmiento, J. L., et al. (2004), Response of ocean ecosystems to climate warming, *Global Biogeochem. Cycles*, *18*, GB3003, doi:10.1029/2003GB002134.

1. Introduction

[2] A wide range of coupled climate models (Atmosphere-Ocean General Circulation Models, or AOGCMs) have been developed in order to investigate the response of

[1]Atmospheric and Oceanic Sciences Program, Princeton University, Princeton, New Jersey, USA.
[2]Duke University, Beaufort, North Carolina, USA.
[3]Laboratoire des Sciences du Climat et de l'Environnement, Unite Mixte de Recherche CEA-CNRS, LSCE, CEA Saclay, Gif-sur-Yvette, France.
[4]Department of Marine Chemistry and Geochemistry, Woods Hole Oceanographic Institution, Woods Hole, Massachusetts, USA.
[5]CSIRO Atmospheric Research, Aspendale, Victoria, Australia.
[6]Climate and Global Dynamics, National Center for Atmospheric Research, Boulder, Colorado, USA.
[7]CSIRO Division of Marine Research, Hobart, Tasmania, Australia.
[8]Max-Planck-Institut für Meteorologie, Hamburg, Germany.
[9]Institute of Physics, St. Petersburg State University, St. Petersburg, Russia.
[10]Met Office, Hadley Centre for Climate Prediction and Research, Bracknell, UK.
[11]Geophysical Fluid Dynamics Laboratory, Princeton, New Jersey, USA.

0886-6236/04/2003GB002134

the physical ocean-atmosphere system to increased greenhouse gases and aerosols [*Cubasch et al.*, 2001]. The primary motivation for the study described in this paper is to examine those aspects of AOGCM simulations that we believe are most relevant to determining how ocean biology will respond to global warming. These simulations of global warming predict oceanic temperature increases; dramatic changes in oceanic stratification, circulation, and convective overturning; and changes in cloud cover and sea ice and thus light supply to the surface ocean. It is very likely that such changes will cause significant alterations in the biology of the oceans [*Denman et al.*, 1996; *Cox et al.*, 2000; *Bopp et al.*, 2001; *Boyd and Doney*, 2002]. Of the three classes of impacts, (1) warming, (2) light supply response to changes in cloudiness and mixed layer thickness, and (3) reduced nutrient supply due to increased vertical stability and reduced vertical exchange, warming and light supply affect photosynthesis directly, while increased stability and reduced vertical exchanges have an influence on ocean ecology through reduced nutrient supply. In addition, an increase in stability will have significant impacts in higher-latitude regions where deep mixing over much of the year presently forces phytoplankton to spend too much time at depths where the light supply is inadequate for photosynthesis. We attempt here to provide an objective measure of the range of responses to climate warming using a suite of relevant model diagnostics for a set of six different warming simulations with AOGCMs.

[3] We chose seven diagnostics to include in this study. The first three are sea surface properties: temperature, salinity, and density. Temperature is important because it directly impacts physiological processes. In addition, we use regional variations in temperature, salinity, and density as indicative of relevant water mass differences. We have in mind particularly such features as colder temperatures associated with processes such as upwelling or deep mixing, which would tend to have high nutrient supply rates; and fresh surface waters, which tend to be associated with high stratification and low nutrient supply (or higher nutrient supply if near river mouths). The next three diagnostics are directly related to nutrient supply to the euphotic zone: upwelling at the model layer that is closest to 50 m, vertical density gradient between the two model layers that span 50 m, and mixed layer depth. The seventh diagnostic is the extent of sea ice cover, since regions covered by sea ice during at least part of the year tend to have a unique ecology that differs from areas that are always ice free. The seasonal productivity cycle in marginal sea ice zones is strongly affected by meltwater during the period of ice retreat. The reduced salinity creates a stable, shallow surface layer that supports a sharp seasonal pulse of primary productivity [*Smith et al.*, 2000; *Hiscock et al.*, 2003].

[4] As the results of the models were analyzed, it became evident that it would be useful to have a biological model that could be used to predict the biological response to the physical changes predicted by the AOGCMs. Among the approaches that can be taken to do this are (1) mechanistic models of marine biology that directly predict the biological response; (2) inferring the response by seeking for climate response patterns in the AOGCMs that are similar to observed modes of interannual variability such as the El Niño/Southern Oscillation or Pacific Decadal Oscillation; and (3) developing empirical models based on observational constraints on the chlorophyll and primary production distributions. Oceanographers have put considerable effort into the first of these three approaches [e.g., *Fasham et al.*, 1990, 1993; *Maier-Reimer*, 1993; *Sarmiento et al.*, 1993; *Aumont et al.*, 1999; *Cox et al.*, 2000; *Bopp et al.*, 2001; *Christian et al.*, 2002a, 2002b; *Moore et al.*, 2002]. However, the mechanistic models used in such studies are still in the early stages of development and are difficult to validate. In addition, while at least two groups have already included biological models in their AOGCMs [*Cox et al.*, 2000; *Friedlingstein et al.*, 2001; *Dufresne et al.*, 2002] and many are working to do so at present, not all have done so, including most of the groups participating in this study. Furthermore, the biological models differ from case to case, which makes it difficult to separate differences in physical responses from differences in biological models. For purposes of this study, we preferred to use a common methodology to estimate the biological response to climate warming.

[5] The second approach of inferring future behavior from interannual variability such as that summarized by *Boyd and Doney* [2002] suffers from the limitation that it can only be applied in situations where the patterns of global warming actually correspond to patterns of interannual variability. The warming pattern associated with increases in greenhouse gases in model simulations has been shown to be quite different from any of the variability modes [*Manabe and Stouffer*, 1996; *Stone et al.*, 2001], although one can see *Corti et al.* [1999] for a different point of view. Even if it turned out that there is a strong correlation between patterns of warming and patterns of interannual variability, none of the AOGCMs considered here do very well at simulating the largest mode of interannual variability, the El Niño/Southern Oscillation [*McAvaney et al.*, 2001].

[6] The approach that we take here is to develop a statistical model based on primary production measurements, the global chlorophyll distribution inferred from satellite color observations, the model variables that we analyze as part of our AOGCM intercomparison exercise, and the observed counterparts to the model variables. This approach, which has a long history, is essentially that advocated by *Platt and Sathyendranath* [1988] (compare synthesis by *Platt and Sathyendranath* [1999]). We use empirically based primary production models that estimate primary production as a function of temperature, light supply, euphotic zone depth, and chlorophyll concentration. The chlorophyll concentration is obtained using a statistical model that we develop here based on a multiple linear regression of the log of the satellite-based global chlorophyll distribution to observed variables. Before regressing the statistical model against the variables, we divide the world into a set of biomes, which are further subdivided into biogeographical provinces within each of which we develop a separate statistical model. The

Table 1. Models Participating in This Study

Group	Model Experiment	References
CSIRO	CSIRO G	*Hirst et al.* [2000], *Matear et al.* [2000]
GFDL	GFDL R15_b	*Dixon et al.* [2003]
HADLEY	HadCM3 GSIO	*Johns et al.* [2003]
IPSL	IPSL-CM2 A2	*Dufresne et al.* [2002]
MPI	ECHAM4/OPYC3 GSIO	*Roeckner et al.* [1999]
NCAR	CSM 1.3 GS	*Boville et al.* [2001], *Dai et al.* [2001]

model-predicted variables from the AOGCM global warming and control simulations are then used to predict the shift in the biogeographical province boundaries, and, within each new biogeographical province, what the future chlorophyll distribution would be. The predicted chlorophyll distributions are then used to calculate the primary production.

[7] The next section provides information on the six AOGCMs used in this study and describes the physical diagnostics obtained as part of this study. This is followed by a section that describes first our proposed biome and biogeographical province classification scheme, then the primary production and statistical chlorophyll models. Subsequent sections describe the climate response results and then discuss the overall findings.

2. Description of Models and Model Diagnostics

[8] Table 1 lists the six coupled climate models (AOGCMs) included in this study and provides references to papers describing them. The nomenclature of the particular AOGCM experiment (second column of Table 1) is based on that given by *Cubasch et al.* [2001]. Table 2 gives a brief description of the six AOGCMs. All the models use the IS92a greenhouse gas radiative forcing scenario [*Leggett et al.*, 1992] except for GFDL, which uses a 1% per year CO_2 increase after 1990 (similar to IS92a) and IPSL, which uses the SRES A2 scenario (also similar to IS92a [*Nakicenovic et al.*, 2000]). All of the models include direct radiative forcing of sulfate aerosols except for CSIRO and IPSL. The HADLEY and MPI models also include indirect forcing of sulfate aerosols as well as forcing from tropospheric ozone changes. Three of the models employ the flux adjustment method for preventing model drift. The shortest simulation, that for MPI, ends in 2049, which limits our analysis of that model to the middle of this century.

[9] Table 3 summarizes a set of climate response variables from those AOGCMs for which they are available [*Cubasch et al.*, 2001], and Figure 1 shows the time history of the global mean surface air temperature for all six models. The "effective equilibrium sensitivity" for a CO_2 doubling ranges from a low of 2.2°C for the NCAR model to a high of 4.2°C for the GFDL R15a model (a predecessor to the R15b model but with similar sensitivity). The IPSL CM-2 AOGCM did not perform the effective equilibrium sensitivity analysis, but the mixed layer ocean equilibrium warming responses given in the next row show that it falls within the range of the other models. The results shown in Figure 1 are broadly consistent with this behavior, although it should be noted that heat storage in the ocean will have an impact on the time evolution shown in the figure [*Raper et al.*, 2002]. This set of AOGCMs is reasonably representative of the overall range of climate responses summarized in the IPCC 2001 Third Assessment Report [*Cubasch et al.*, 2001].

[10] The sea surface temperature, salinity, and density diagnostics are all obtained from the uppermost layer of each model. The upwelling is from the model layer that is closest to 50 m (see Table 4 for actual depths). The vertical density gradient is calculated between the two model layers whose interface is closest to 50 m (see Table 4). The mixed layer depth is defined as the depth at which σ_θ is 0.1 units above the surface value, except in the MPI model, where it is given by a prognostic mixed layer model. The seven diagnostics, including the sea ice cover extent, were

Table 2. Description of Model Simulations

Group	Scenario	Resolution[a]	Horizontal Mixing Scheme[b]	Flux Adjustment	Starting and Final Year
CSIRO	historical equivalent CO_2 to 1990 then IS92a to 2082 and constant thereafter	3.2 × 5.6 L21	G-M	yes	1881–2100
GFDL	historical equivalent CO_2 to 1990 then 1% CO_2 (approx IS92a) + direct effect of sulfate aerosols	4.5 × 3.7 L12	isopycnal + Horizontal background	yes	1866–2095
HADLEY	historical greenhouse gases to 1990, then IS92a + direct + indirect effect of sulfate aerosols + tropospheric ozone changes	1.25 × 1.25 L20	G-M	no	1860–2100
IPSL	CO_2 emissions: historical to 1990 then SRES A2 scenario (http://ipcc-ddc.cru.uea.ac.uk/cru_data/examine/emissions/SRES98a2.html)	2.5 × 4 L31	isopycnal	no	1860–2100
MPI	historical greenhouse gases to 1990, then IS92a direct + indirect effect of sulfate aerosols + ozone changes	2.8 × 2.8 L11	isopycnal with diffusion of layer thickness	yes	1860–2049
NCAR	historical greenhouse gases to 1990, then approximately IS92a + direct effect of sulfate aerosols	2.0 × 2.4 L45	G-M	no	1870–2100

[a]Resolutions given are for the ocean component of each climate model. The horizontal resolution is expressed as degrees latitude versus degrees longitude. The vertical resolution is expressed as Lmm, where mm is the number of vertical layers.

[b]Horizontal mixing schemes are for the ocean component of each climate model and include isopycnally oriented mixing, geodesic coordinate mixing (i.e., horizontal), and G-M mixing as described by *Gent and McWilliams* [1990]. The MPI ocean is an isopycnic coordinate model.

Table 3. Climate Sensitivity of Participating Models in °C

	CSIRO	GFDL	HADLEY	IPSL	MPI	NCAR
	Mk2	R15a	HadCM3	CM−2	ECHAM4/OPYC	CSM1.3
Effective climate sensitivity[a]	3.7	4.2	3.0		2.6	2.2
Mixed layer ocean equilibrium warming[b]	4.3	3.7	3.3	3.6		

[a]Effective climate sensitivity is a measure of the strength of feedbacks to 2 × CO_2 at a particular time when the model is continuing to warm (see *Cubasch et al.* [2001] for a detailed explanation). It would equal the 2 × CO_2 sensitivity if the model were in equilibrium.
[b]Mixed layer ocean equilibrium warming is the warming that the atmospheric model gives in response to 2 × CO_2 when coupled to a mixed layer ocean.

obtained on a month-by-month basis. However, in what follows we make use of primarily the annual mean results averaged over the 21-year period between 2040 and 2060. The only exception is the MPI model, for which we use averages over the 10-year period from 2040 to 2049, when their simulation ends. We also show some results averaged over the period 2080 to 2100. Most of the model diagnostics shown throughout this paper will be the average change, Δ, defined as the warming simulation minus the control climate simulation.

3. Model Analysis Methods

3.1. Biomes and Biogeographical Provinces

[11] Comparison of global data sets on the abundance of phytoplankton biomass (see Figure 2a, showing chlorophyll estimated from Sea-viewing Wide Field-of-view Sensor (SeaWiFS) color observations by J. Yoder and M. Kennelly (US JGOFS SMP data: Global SeaWiFS chlorophyll, 2001, available at http://usjgofs.whoi.edu/las/jglas.html?dset=Global+SeaWiFS+chlorophyll+1998-2000) (hereinafter referred to as Yoder and Kennelly, online data set, 2001)), with physical parameters such as upwelling and wintertime mixing suggests the possibility of dividing the ocean into major biomes based on physical characteristics. Such a dynamical approach to defining biomes, which is analogous to that adopted by *Longhurst* [1994], makes it possible to use predictions of climate change models to estimate how biome boundaries might change in response to climate warming [*Boyd and Doney*, 2002]. Some of the obvious features in the chlorophyll distribution include the tropics, where high chlorophyll is associated with equatorial and coastal upwelling regions. Poleward of the equatorial regions are the low biomass regions of the permanently stratified subtropical gyres, followed at higher latitudes by the high biomass regions of the poleward half of the subtropical gyres, the subpolar gyres, and the marginal sea ice zone. As *Barber* [1992] discusses, the best way to account for these fundamentally different biomes is that there are differences in the large scale physical processes that control nutrient supply [cf. *Sverdrup*, 1955; *Reid et al.*, 1978; *Gargett*, 1998]. Neither temperature nor light supply alone or in combination can account for the observed patterns in the annual mean chlorophyll distribution.

[12] The starting point for our analysis of the model variables is to define a set of geographic regions, which we shall refer to as biomes, based on a set of physical criteria of nutrient supply rate. Nutrients are generally

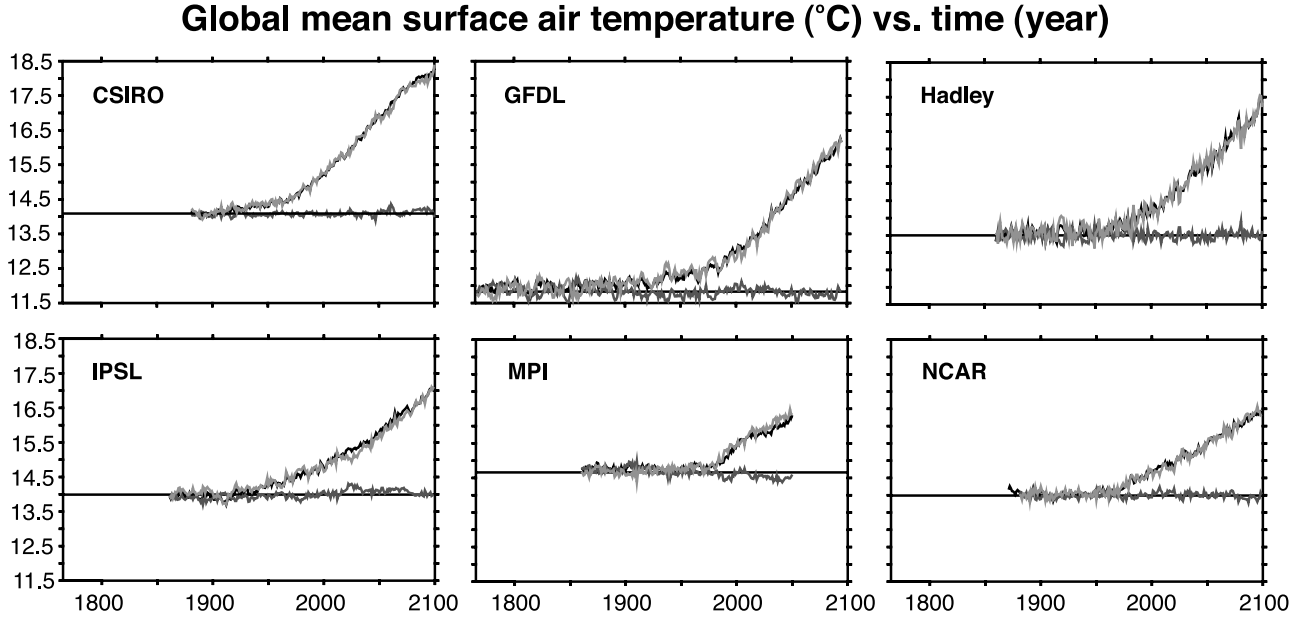

Figure 1. Time-dependent plots of mean surface air temperature for all six coupled climate models. The red line is the control scenario, the green line is the climate warming scenario, and the black line is the climate warming scenario minus the control scenario. See color version of this figure at back of this issue.

Table 4. Calculation of Derived Quantities[a]

Group	Upwelling Depth, m	Vertical Density Gradient
CSIRO	37.5	$\frac{\sigma_\theta(65\text{ m})-\sigma_\theta(37.5\text{ m})}{27.5\text{ m}}$
GFDL	24.45	$\frac{\sigma_\theta(85.1\text{ m})-\sigma_\theta(24.45\text{ m})}{60.65\text{ m}}$
HADLEY	47.8	$\frac{\sigma_\theta(67\text{ m})-\sigma_\theta(47.8\text{ m})}{19.2\text{ m}}$
IPSL	50	$\frac{\sigma_\theta(55\text{ m})-\sigma_\theta(45\text{ m})}{10\text{ m}}$
MPI	100	$\frac{\sigma_\theta(100\text{ m})-\sigma_\theta(0\text{ m})}{100\text{ m}}$
NCAR	43.75	$\frac{\sigma_\theta(56.755\text{ m})-\sigma_\theta(43.75\text{ m})}{13.005\text{ m}}$

[a]Upwelling was determined at the model layer interface that was closest to 50 m. In the case of the MPI model, the depth represents not the resolution of the model, but rather the depth to which this particular diagnostic was interpolated and then saved when the model was run. The annual mean vertical density gradient was calculated by averaging monthly gradients.

depleted or nearly depleted in the surface waters and rich within the thermocline when there is sufficient light. Lower biological productivity will thus generally be associated with downwelling velocities and weak vertical mixing and convection. Higher biological productivity requires upwelling and strong vertical mixing and convection in order to supply nutrients. We thus define our model-based biomes using the sign of the vertical velocity (i.e., whether the water is upwelling or downwelling) at the model layer nearest to 50 m, and the maximum wintertime mixed layer depth as defined in Table 4, which we take as an indicator of the extent of vertical mixing and convection. We also define a corresponding observationally based set of biomes using the maximum wintertime mixed layer depth estimates of

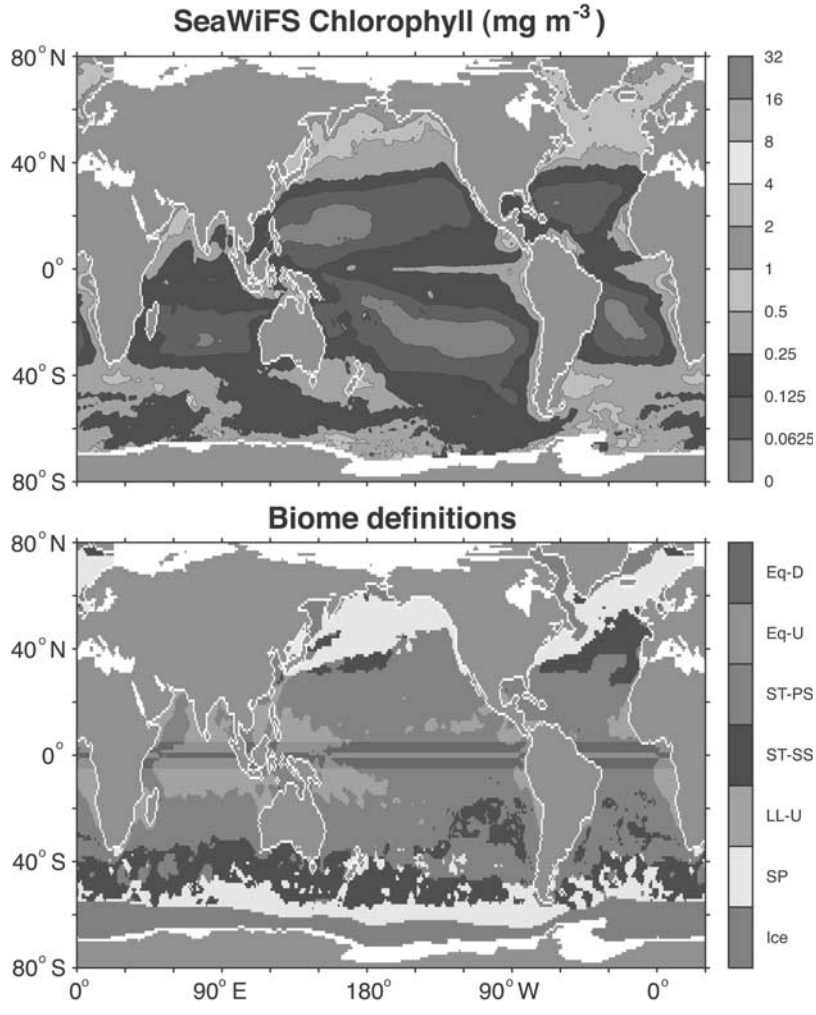

Figure 2. (a) Annual mean SeaWiFS chlorophyll from Yoder and Kennelly (online data set, 2001). (b) Biome classification scheme calculated using mixed layer depths obtained from observed density and from upwelling calculated from the wind stress divergence using observed winds. The equatorially influenced biome covers the area between 5°S and 5°N, and is colored a dirty light blue in areas where upwelling occurs (labeled "Eq-U" on the color bar) and dark pink in areas where downwelling occurs (labeled "Eq-D"). Outside of this band, the region labeled "Ice" (red) is the marginal sea ice biome, the region labeled "SP" (yellow) is the subpolar biome, the region labeled "LL-U" (light blue) is the low-latitude upwelling biome, the region labeled "ST-SS" (dark blue) is the seasonally mixed subtropical gyre biome, and the region labeled "ST-PS" (pink) is the permanently stratified subtropical gyre biome. See color version of this figure at back of this issue.

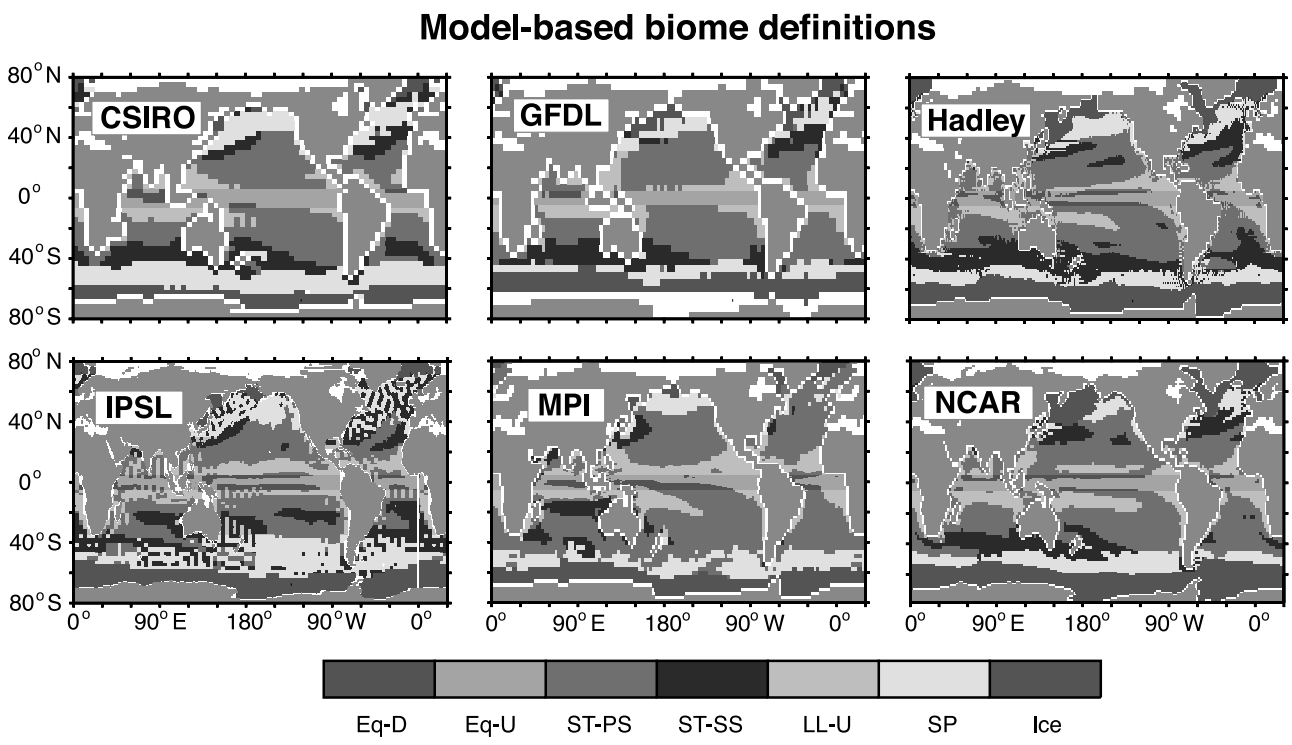

Figure 3. Biome classifications as determined from the AOGCM control climate variables for each of the six models. The color scheme and symbols are described in the Figure 2 caption. See color version of this figure at back of this issue.

Levitus et al. [1998] and w obtained using the Ekman divergence calculated with the winds of *Hellerman and Rosenstein* [1983].

[13] The two variables we use to define the biomes have the virtue of simplicity, but they do not consider the influence of light supply, which is important in high latitudes, and of airborne supply of micronutrients and macronutrients such as iron, which is important in the North and equatorial Pacific, as well as the Southern Ocean. These additional factors are accounted for indirectly by separating the biomes into biogeographical provinces (e.g., the North Pacific subpolar gyre), which are allowed to differ from other provinces in the same biome.

[14] We define an equatorially influenced biome as covering the latitude band between 5°S and 5°N where strong equatorial upwelling accompanied by lateral transport into regions of downwelling is a dominant factor in determining where high biological productivity occurs (see Figures 2b and 3). The equatorially influenced biome is subdivided into two biogeographical provinces according to whether the vertical velocity is upward or downward (in other words, on the basis of the sign of the vertical velocity, not its magnitude), and further subdivided by basin. From the observationally based biome areas shown in Figure 2b and Table 5, we calculate that the equatorially influenced biome takes up 10% of the surface ocean area, of which 60% is in the upwelling provinces and 40% is in the downwelling provinces. Because of the low horizontal resolution of many of the AOGCMs, the upwelling provinces occupy an average of 75% of the equatorially influenced biome in the control simulations, with the remainder in the downwelling provinces (see Figure 3 and Table 6). The SeaWiFS average chlorophyll in this biome is 0.21 mg m^{-3} in upwelling regions and 0.21 mg m^{-3} in downwelling regions (Table 5).

[15] Poleward of the equatorially influenced biome, the SeaWiFS chlorophyll shown in Figure 2a rises from a low of less than 0.1 mg m^{-3} in the subtropics to a high in excess 1.0 mg m^{-3} in the high latitudes of the Northern Hemisphere, and 0.4 mg m^{-3} in the high latitudes of the Southern Hemisphere (compare Table 5). The lowest surface chlorophyll concentrations occur in the permanently stratified regions of the subtropical gyres often referred to as the oligotrophic gyres. These are areas characterized by downwelling and shallow wintertime mixed layers, which together limit the supply of nutrients from the thermocline. We define a permanently stratified subtropical biome as the region where the annual mean vertical velocity at 50 m is downward and the maximum wintertime mixed layer depth never exceeds 150 m. This is by far the largest biome, occupying 45% of the ocean area as defined by observations (see Figure 2b and Table 5), and a mean of 38% as defined by the average of the AOGCM control climate simulations (see Figure 3 and Table 6). SeaWiFS chlorophyll concentration averages 0.14 mg m^{-3} in the Northern Hemisphere, and 0.13 mg m^{-3} in the Southern Hemisphere (Table 5).

[16] A seasonally mixed subtropical biome of intermediate chlorophyll concentrations (average = 0.31 mg m^{-3} in the Northern Hemisphere and 0.21 mg m^{-3} in the southern hemisphere; Table 5) is defined as also having a downward

Table 5. Total Area of Biogeographical Provinces Determined From Observations, and Geometric Mean SeaWiFS Chlorophyll Within Each Province

	Area, $\times 10^{12}$ m^{-2}				Chlorophyll, mg m^{-3}			
	Indian	Pacific	Atlantic	Global	Indian	Pacific	Atlantic	Global
			Northern Hemisphere					
Marginal sea ice		1.2	1.9	3.1		1.28	0.97	1.05
Subpolar		12.3	7.6	19.9		0.57	0.71	0.63
Subtropical seasonal		2.8	7.3	10.1		0.31	0.31	0.31
Subtropical permanent	3.1	41.7	18.3	63.1	0.37	0.12	0.16	0.14
Low-latitude upwelling	3.7	8.6	2.3	14.6	0.41	0.13	0.39	0.21
			5°S to 5°N					
Upwelling	4.6	6.4	2.0	12.9	0.17	0.20	0.40	0.21
Downwelling	2.1	12.8	4.5	19.3	0.20	0.20	0.24	0.21
			Southern Hemisphere					
Low-latitude upwelling	9.3	6.4	2.2	18.0	0.16	0.13	0.55	0.17
Subtropical permanent	20.2	43.4	18.6	82.2	0.14	0.11	0.16	0.13
Subtropical seasonal	15.7	17.5	8.0	41.1	0.25	0.15	0.26	0.21
Subpolar	7.1	9.4	4.7	21.1	0.24	0.22	0.36	0.25
Marginal sea ice	5.9	4.7	5.5	16.2	0.25	0.34	0.38	0.32
Total	71.7	167.0	82.9	321.6				

vertical velocity, but with wintertime mixed layers exceeding 150 m. A mixed layer of >150 m is generally deep enough to penetrate into the high nutrient waters of the thermocline. The seasonally mixed subtropical biome accounts for 16% of the ocean area as defined by the observations (see Figure 2b and Table 5), 15% as defined by the AOGCM control climate simulations (see Figure 3 and Table 6).

[17] In roughly the same latitude band as the subtropical gyres, there are also regions of upwelling that occur primarily along the western margins of the continents. These are regions of high nutrient supply and thus high biological productivity, and which sustain some of the major fisheries of the world. In order to account for these regions, we define a low-latitude upwelling biome as the region where upwelling occurs between 35°S and 30°N, but not including the equatorially influenced biome. The chlorophyll in this biome averages 0.21 mg m^{-3} in the Northern Hemisphere, and 0.17 mg m^{-3} in the Southern Hemisphere (Table 5). Note that our definition of the low-latitude upwelling biome is not entirely successful, in that it includes large areas in the western Pacific and central and eastern Indian Ocean where upwelling occurs but biological productivity is extremely low. A major contributor to this problem is the presence in these regions of the fresh barrier layer at the base of the mixed layer, which prevents access

Table 6. Average Response of Biogeographical Province Areas to Global Warming Averaged Over the Period 2040 to 2060[a]

	Indian Ocean			Pacific Ocean			Atlantic Ocean			Global		
	Control	Δ	%Δ	Control	Δ	%Δ	Control	Δ	%Δ	Control	Δ	%Δ
					Northern Hemisphere							
Marginal sea ice				3.8	−1.7	−45.3	3.2	−1.2	−37.5	7.0	−2.9	−41.7
Subpolar				8.5	1.2	13.9	5.5	1.1	19.7	14.0	2.3	16.2
Subtropical seasonal				4.9	−0.7	−13.4	8.8	−0.8	−9.4	13.6	−1.5	−10.9
Subtropical permanent	3.3	0.1	2.3	35.4	1.0	2.9	12.5	0.9	7.4	51.2	2.0	4.0
Low-latitude upwelling	2.1	−0.1	−6.8	10.9	0.2	1.6	4.4	0.0	0.8	17.3	0.1	0.4
					5°S to 5°N							
Upwelling	4.5	0.5	10.1	14.6	0.2	1.3	4.6	0.1	2.4	23.7	0.7	3.2
Downwelling	2.3	−0.5	−19.5	4.4	−0.2	−4.3	1.3	−0.1	−10.9	7.7	−0.8	−9.7
					Southern Hemisphere							
Low-latitude upwelling	7.9	−0.1	−0.7	8.7	−0.6	−7.3	3.8	0.2	4.8	20.4	−0.5	−2.5
Subtropical Permanent	15.0	1.1	7.3	37.4	3.6	9.7	13.9	1.5	10.8	66.3	6.2	9.4
Subtropical seasonal	13.8	−0.5	−3.3	12.1	−1.8	−14.7	6.4	−1.2	−18.4	32.3	−3.4	−10.6
Subpolar	8.2	1.5	18.7	12.5	0.4	3.3	7.1	0.2	3.4	27.8	2.2	7.9
Marginal sea ice	8.8	−2.1	−23.7	8.8	−1.5	−16.9	7.8	−0.8	−10.3	25.3	−4.4	−17.2
Total	65.8			161.9			79.3			306.7		

[a]Areas are given in 10^{12} m^2. Δ is the difference between the model average warming minus control; %Δ is the per cent change of the averages shown in the table. The averages are taken over all the AOGCMs except MPI, which was not included because its prognostic mixed layer generally gives much shallower mixed layers than the potential density-dependent definition used by the remaining models. The basin and global totals of the control simulation are smaller than the observed areas due to the coarse grid resolution of the models. There is no Atlantic downwelling province in the GFDL model. The following provinces disappear in the warming scenarios: Pacific downwelling in the GFDL model, Southern Hemisphere Atlantic subtropical seasonal in the GFDL model, and Northern Hemisphere Pacific marginal sea ice in the CSIRO model.

to the deep cold waters below [*Sprintall and Tomczak*, 1992]. This biome accounts for 10% of the ocean area as defined by observations (see Figure 2b and Table 5) and 12% as defined by the AOGCM control climate (see Figure 3 and Table 6).

[18] Next, we define a subpolar biome as the regions north of 30°N and south of 35°S where there is net annual mean divergent flow at the surface of the ocean, i.e., where upwelling occurs. The Northern Hemisphere subpolar biome has a mean chlorophyll concentration of 0.63 mg m^{-3}, and the Southern Hemisphere subpolar biome has one of 0.25 mg m^{-3} (Table 5). The lower chlorophyll concentrations of the Southern Hemisphere have been explained as resulting from iron limitation [*Helbling et al.*, 1991; *Martin et al.*, 1991; *de Baar et al.*, 1995; *Boyd et al.*, 1999; *de Baar et al.*, 1999; *Boyd et al.*, 2000; *Boyd*, 2002]. The subpolar biome occupies 13% of the world ocean area as defined by the observations (see Figure 2b and Table 5), and 14% as defined by the AOGCM control climate simulations (see Figure 3 and Table 6).

[19] Finally, we define a marginal sea ice biome that is covered by sea ice during some part of the year. This biome occupies 6% of the world area (most of which is in the Southern Hemisphere) in the observationally based analysis of Table 5 (which uses the *Alexander and Mobley* [1976] ice pack limits), and 11% in the AOGCM based analysis of Table 6 (see also Figures 2b and 3, respectively). The marginal sea ice biome has average chlorophyll concentrations of 1.05 mg m^{-3} in the Northern Hemisphere, and 0.32 mg m^{-3} in the iron-impoverished Southern Hemisphere.

[20] A comparison of our biome definitions with those of *Longhurst* [1994] shows a strong correspondence. The Longhurst polar biome corresponds to our marginal sea ice biome, his westerlies biome corresponds to the combination of our seasonally mixed subtropical and subpolar biomes, and his trades biome corresponds to a combination of our permanently stratified subtropical and equatorially influenced biomes. In addition, our low-latitude upwelling biome is a subset of the Longhurst coastal boundary zone biome.

[21] A comparison of the geographical distribution of our biomes with the observed chlorophyll distribution (Figure 2) shows a strong correlation, but with some differences that we attribute primarily to the influence of airborne iron supply on production, particularly in the Southern Ocean. We attempt to account for the influence of continental proximity and wind patterns on the iron supply, as well as for large-scale oceanographic differences such as the strong stratification of the North Pacific due to the steep halocline, by further dividing the biomes defined above into "biogeographical provinces." This subdivision includes the three ocean basins (Atlantic, Pacific, and Indian) and the Northern and Southern Hemispheres (except for the equatorially influenced biome, which is not divided by hemisphere). Overall, we have 12 biogeographical provinces in the Atlantic and Pacific Oceans, and nine in the Indian Ocean (which is missing the Northern Hemisphere seasonally mixed subtropical, subpolar, and marginal sea ice biomes) giving a total of 33 biogeographical provinces.

[22] To summarize, the sequence we follow in defining the geographical extent of the biomes and biogeographical provinces is as follows: (1) Define the equatorially influenced biome as the latitude band between 5°S and 5°N and divide this into upwelling and downwelling provinces. (2) Exclude all regions that are permanently covered by sea ice from the classification. Define all areas covered by sea ice during part of the year as marginal sea ice biomes. (3) Define as permanently stratified subtropical biomes those regions where downwelling occurs and the maximum mixed layer depth MML (based on monthly analyses) is $\leq$150 m. (4) Define the seasonally stratified subtropical biome as those regions where downwelling occurs but the MML is >150 m. Note from Figures 2 and 3 that this includes a few small areas in high latitudes that are embedded within the subpolar biome. (5) Define all upwelling regions between 35°S and 30°N as low latitude upwelling biomes. (6) Define all upwelling regions north of 30°N and south of 35°S as subpolar biomes. In addition, we exclude marginal bodies of water such as the Mediterranean Sea, Baltic Sea, Red Sea, Gulf of Oman, and Hudson Bay, and we exclude all of the Arctic north of 67°N except for the extension of the North Atlantic to 80°N bounded by 80°W and 23°E. The separation of biomes into biogeographical provinces is made by dividing Northern Hemisphere from Southern Hemisphere (except for the equatorially influenced biome) and by dividing the Atlantic from the Indian Ocean at 19°E, the Indian from the Pacific at 150°E, and the Pacific from the Atlantic at 71°W.

3.2. Primary Production Algorithms

[23] To estimate how the physical changes that occur in response to climate warming will affect primary production in the ocean, we make use of three phytoplankton primary productivity algorithms developed by *Behrenfeld and Falkowski* [1997], *Carr* [2002], and *Lee et al.* [1996] as implemented by *Marra et al.* [2003] (compare *Campbell et al.* [2002] round-robin comparison study). These algorithms estimate primary production as a function of the surface chlorophyll content, light supply, and temperature, and some measure of vertical light attenuation and the vertical chlorophyll distribution. The most important difference between these models that is of relevance to this paper is in the dependence of their chlorophyll normalized primary production on temperature. As illustrated in Figure 4a, the *Behrenfeld and Falkowski* [1997] model shows an increase with temperature to a maximum at 20°C, and a decrease thereafter that the authors attribute to the association between high temperatures and strong vertical stratification leading to nutrient limitation. The other two models show a more continuous increase at all temperatures, but with significant differences between them. As might be expected, the difference in temperature sensitivity between these algorithms has a major impact both on estimates of the present primary production (Figure 4b) and on the estimated response of primary production to global warming that we show below. The fact that the temperature sensitivity may in some cases, such as in the *Behrenfeld and Falkowski* [1997] algorithm, be parameterizing nutrient limitation rather than

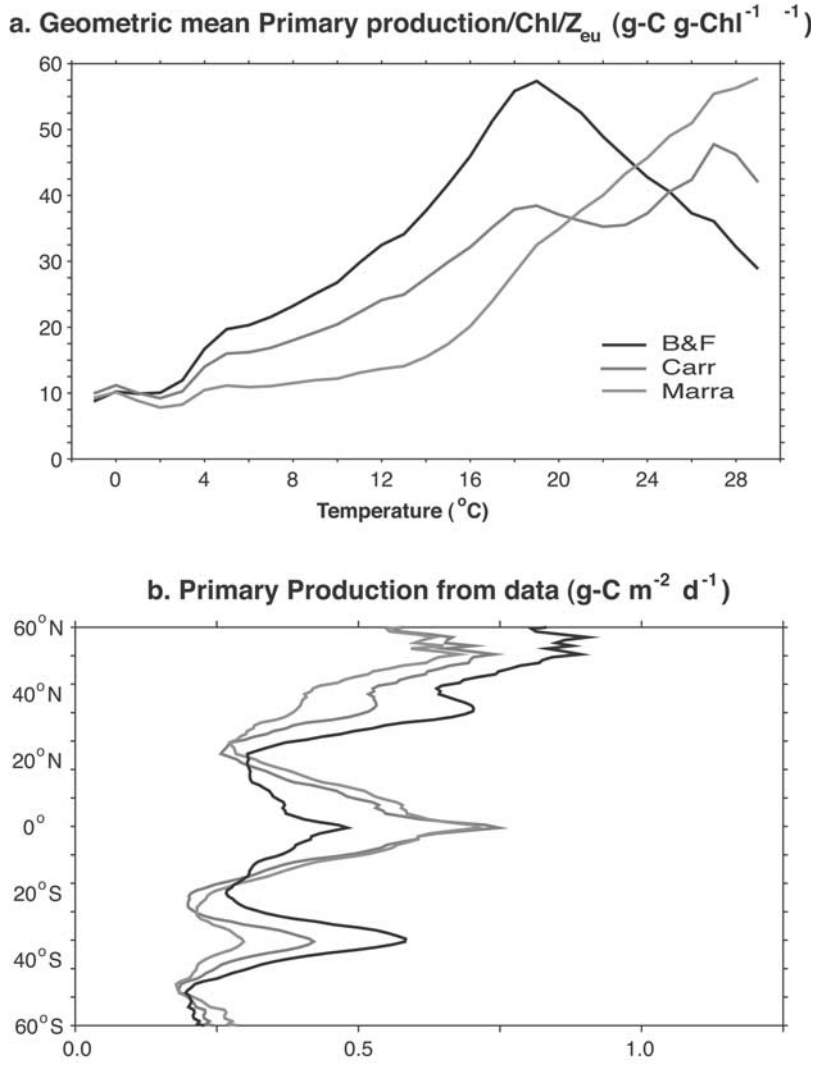

Figure 4. Primary production derived from SeaWiFS chlorophyll and observed light and temperature using the *Behrenfeld and Falkowski* [1997], *Carr* [2002], and *Marra et al.* [2003] algorithms (B&F, Carr, and Marra, respectively). (a) Primary production normalized by chlorophyll and euphotic zone depth (Z_{eu}) and then binned and averaged in 1°C bins. Z_{eu} is derived from the implied vertical distribution of chlorophyll as part of the three primary production algorithms. (b) Zonal mean primary production. See color version of this figure at back of this issue.

the actual temperature response of metabolic processes complicates the interpretation of the primary production response calculated with these algorithms.

3.3. Empirical Chlorophyll Model

[24] The use of an oceanic empirical model for estimating chlorophyll is analogous to the use of biome-based empirical models to determine the long-term response of terrestrial ecosystems to climate change [e.g., *Potter et al.*, 1993; *Schimel et al.*, 2000]. In this approach, climate and other variables that are associated with a given land biome are identified and used to project the potential vegetation under global warming. A limitation of this approach on land is that the shift of a given biome to a new location may take decades to centuries due to the limited spatial extent of seed dispersal and long timescale of land ecosystem turnover. The oceans suffer less from these limitations because of the relatively rapid dispersal of seed populations by ocean circulation, and because planktonic ecosystems have turnover times of days to weeks.

[25] We define a separate empirical chlorophyll model for each of the 33 biogeographical provinces. Every model is obtained by a stepwise multiple linear regression (MLR) of the log of the SeaWiFS chlorophyll distribution CHL normalized to 1 mg m^{-3} to a set of n observed variables V_i

$$\ln(\mathrm{CHL}_j) = a_{0,j} + \sum_{i=1}^{n} a_{i,j} \times V_i, \qquad (1)$$

where $j = 1, 33$ is a given biogeographical province and the $a_{i,j}$'s are parameters obtained by the MLR. We use the log of chlorophyll because chlorophyll is lognormally distributed [*Campbell*, 1995]. Since we wish to apply equation (1) to the climate model simulations, our choice of variables is limited to those diagnostics that we obtain from the climate models as part of this study, namely, the sea-surface temperature SST, salinity SSS, and density $SS\sigma_\theta$ the mixed layer depth (we use only the maximum winter mixed layer depth MML); vertical velocity w; and the vertical density gradient. We do not include sea ice extent because this is already used to define one of the biomes. An additional variable we consider is the growing season length GSL, defined as the number of days that the light supply at a given location exceeds 5 Einsteins per day per m^2 and the mixed layer is shallower than 100 m. The 100-m-depth cutoff is chosen because this is the nominal depth of the 1% light level in clear water below which phytoplankton generally have difficulty obtaining enough light to survive.

[26] The observed values we used for SST, SSS, $SS\sigma_\theta$ and the vertical density gradient at 50 m were taken from *Levitus et al.* [1994a, 1994b]; MML was taken from *Levitus et al.* [1998]; w was obtained using the Ekman divergence calculated with the winds of *Hellerman and Rosenstein* [1983]; and the light supply used to calculate GSL was taken from *Bishop and Rossow* [1991] and *Bishop et al.* [1997]. In doing the fits, we used the actual magnitude of MML, w, density gradient, and GSL. We think of these as tracers of the vertical nutrient supply rate in which the scale of the term is important. For the other three variables, we used only the spatial anomalies within each biogeographical province defined as $SST' = \underline{SST} - \overline{SST}$, $SSS' = SSS - \overline{SSS}$, and $SS\ \sigma'_\theta = SS\sigma_\theta - \overline{SS\sigma_\theta}$, with the overbar denoting the average within the province. We consider the latter three variables to be water mass tracers, having in mind such features as areas of colder temperatures within a biogeographical province being indicative of regions where stronger upwelling and/or deep mixing is bringing nutrients to the surface, or low surface salinity areas indicating the likelihood of strong stratification. Our approach assumes that variations in the absolute magnitude of temperature, salinity, and density are not significant in determining the chlorophyll concentration. This is perhaps not unreasonable with respect to salinity and density, but more controversial in the case of temperature. In effect, we assume that the primary determinant of chlorophyll concentration is nutrient supply, with the temperature dependence of photosynthesis being counterbalanced by a corresponding temperature dependence of the grazing and other loss rates.

[27] After an extensive series of tests we found that SST' and $SS\sigma'_\theta$ carried largely redundant information that frequently led to dipolar behavior in the fits of these two variables to the observations. We thus eliminated $SS\sigma'_\theta$ from our set of variables. More surprising was the finding that variations within each biome of the vertical velocity and vertical density gradient also did not contribute significantly to the MLR regression within each biome. Recall that the sign of the vertical velocity is used in defining the biomes. However, the variation within each biome does not correlate well with the chlorophyll within the biome. It would be useful to investigate this further using higher-resolution satellite-based wind products and including seasonal resolution in the empirical models, which we did not do. Arguably, the effect of the vertical density gradient on nutrient supply is better captured by other variables such as MML. Elimination of these three variables gave a more robust model and reduced the global variance captured by the model (as measured by R-squared) by only a modest amount from 0.83 with all the variables to 0.79 with the reduced set of four variables. Our final empirical model for region j is thus

$$\ln(\mathrm{CHL}_j) = a_{0,j} + a_{1,j} \times \mathrm{SST}'_j + a_{2,j} \times \mathrm{SSS}'_j + a_{3,j} \times \mathrm{MML}_j + a_{4,j} \times \mathrm{GSL}_j. \quad (2)$$

The parameter values and R-squared obtained by the MLR in each biogeographical province are given in Table 7.

[28] In what follows, we use the empirical model defined by equation (2) to calculate chlorophyll from the global warming simulation variables and subtract these from the control chlorophyll calculation in order to predict how the chlorophyll might respond to global warming. This approach has the advantage that it can be applied to any climate warming simulation from a given AOGCM without requiring the incorporation of an ecosystem model. In addition, such an empirical model should, in principle, account for all the complex biological processes that determine the chlorophyll distribution, since the chlorophyll data used to develop the empirical model contain this information within them. However, it is important to be aware of the danger of extrapolating the model beyond the range it is developed for, and to keep in mind that the simple functional form we chose is not always capable of representing the behavior of the system within the bounds of the data. In particular, we note that while the global R-squared is 0.79, there are 12 out of the 33 biogeographical provinces where R-squared is less than 0.50, and five where it is less than 0.25 (the marginal sea ice provinces in the North and South Atlantic, the South Pacific subpolar gyre province, the South Pacific permanently stratified subtropical gyre province, and the South Indian seasonally mixed subtropical gyre province).

3.4. A Note on Seasonality

[29] We focus our analysis of model simulations and observations primarily on annual means. However, we do include some information on seasonality obtained from our month-by-month model and observational diagnostics. For example, our biome and biogeographical province boundaries do not vary with season, but their geographical extent, in addition to being determined by the annual mean vertical velocity, is based on seasonal information about the mixed layer in that we use the maximum mixed layer depth MML to define the boundary between the permanently and seasonally stratified biomes. In addition, the marginal sea ice biome is defined as the area of open ocean that is covered

Table 7. Parameters Obtained by Stepwise Multiple Linear Regressions of Equation (2) to SeaWiFS-Based Chlorophyll Observations for the Biomes Defined as in Section 3.1 Using Observations as Described in Section 3.3[a]

	a_0, unitless	a_1, $°C^{-1}$	a_2, PSU^{-1}	a_3, m^{-1}	a_4, d^{-1}	R^2
			Indian Ocean			
Northern Hemisphere						
Subtropical permanent	−0.714	−0.567	0.056	−0.01004	-	0.73
Low-latitude upwelling	−0.344	−0.550	0.147	−0.02835	-	0.80
5°S to 5°N						
Upwelling	−2.072	−0.435	−0.184	0.01182	-	0.41
Downwelling	−1.344	−0.420	−0.126	−0.00924	-	0.76
Southern Hemisphere						
Low-latitude upwelling	−0.902	−0.187	−0.353	−0.03183	-	0.39
Subtropical permanent	−1.496	−0.058	−0.498	−0.01186	-	0.46
Subtropical seasonal	−1.430	0.028	−0.349	−0.00063	0.00054	0.10
Subpolar	−1.244	0.033	-	−0.00110	−0.00034	0.24
Marginal sea ice	−1.118	−0.080	2.051	−0.00203	−0.00128	0.26
			Pacific Ocean			
Northern Hemisphere						
Marginal sea ice	1.679	0.080	−0.277	−0.00419	−0.00648	0.54
Subpolar	1.163	−0.066	0.106	−0.01698	−0.00297	0.72
Subtropical seasonal	−0.986	−0.013	−0.714	−0.00333	-	0.86
Subtropical permanent	−1.327	−0.077	−0.365	−0.02063	-	0.68
Low-latitude upwelling	−0.973	−0.321	-	−0.04133	-	0.79
5°S to 5°N						
Upwelling	−1.996	−0.235	−0.324	0.01432	-	0.59
Downwelling	−1.687	−0.108	−0.227	0.00245	-	0.53
Southern Hemisphere						
Low-latitude upwelling	−0.797	−0.136	−0.376	−0.03955	-	0.77
Subtropical permanent	−1.218	−0.038	0.620	−0.00119	−0.00066	0.20
Subtropical seasonal	−2.400	−0.172	0.385	−0.00162	0.00280	0.58
Subpolar	−2.265	0.004	−0.377	0.00144	-	0.16
Marginal sea ice	−0.723	−0.128	1.514	−0.00428	−0.00085	0.32
			Atlantic Ocean			
Northern Hemisphere						
Marginal sea ice	0.049	-	-	0	−0.00077	0.02
Subpolar	0.070	−0.034	−0.218	−0.00089	−0.00163	0.66
Subtropical seasonal	−1.273	-	−1.008	-	-	0.88
Subtropical permanent	−1.394	−0.068	−0.364	−0.01302	-	0.60
Low-latitude upwelling	−0.432	−0.464	−0.595	−0.02900	-	0.87
5°S to 5°N						
Upwelling	−0.521	−0.640	−0.196	−0.02316	-	0.88
Downwelling	−1.424	−0.358	−0.738	-	-	0.81
Southern Hemisphere						
Low-latitude upwelling	−0.471	−0.059	−1.341	−0.00603	-	0.76
Subtropical permanent	−1.619	0.011	−0.948	−0.00578	-	0.81
Subtropical seasonal	−2.467	0.014	−0.941	-	0.00464	0.67
Subpolar	−0.179	0.068	−0.744	−0.00626	−0.00080	0.41
Marginal sea ice	−0.523	0.215	-	−0.00212	−0.00287	0.12

[a]A dash indicates that the particular variable did not contribute significantly to the goodness of the fit.

by sea ice part of the year and free of sea ice during part of the year. The mean properties of this and all biomes are for all 12 months of the year for which data are available, but there are many months, especially for the SeaWiFS chlorophyll data in the marginal sea ice zone during periods when the water is covered by ice, when there are no data. In determining the primary production, we use annual mean temperature, chlorophyll, and light supply. On the other hand, our empirical model for chlorophyll uses four variables, two of which are based on our month-by-month model and observational diagnostics, namely the MML and growing season length GSL. One of us, J. L. S., is currently exploring how additional information might be obtained from the month-by-month analyses that would improve our understanding of the present behavior of the system and its potential response to global warming.

4. Response to Global Warming

4.1. Ocean Circulation

[30] Figure 5 shows the zonal mean response to climate warming of the seven diagnostics plus the GSL. As expected, the sea surface temperature warms everywhere (Figure 5a), with the range between models (NCAR lowest and GFDL and CSIRO highest) reflecting the effective equilibrium sensitivity shown in Table 3. The higher south-

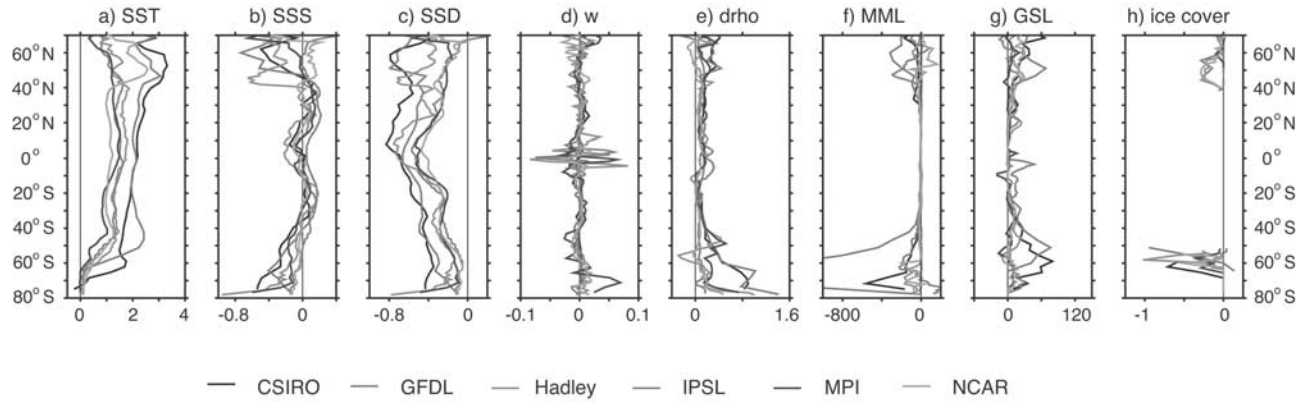

Figure 5. Zonal mean response to climate change (warming minus control) averaged over the period 2040 to 2060 (except for MPI, which is for the period 2040 to 2049) of (a) sea surface temperature, SST in °C, (b) sea surface salinity, SSS in practical salinity units (PSU), (c) sea surface potential density, SSD ($\sigma_\theta \equiv \rho - 1000$ kg m^{-3}), (d) upwelling velocity, w, in m d^{-1}, (e) the fractional change in the vertical density gradient, drho, (f) the wintertime maximum mixed layer depth, MML, in m, (g) the growing season length, GSL, in days, and (h) the ocean area of maximum wintertime sea ice extent in 10^{12} m^2 per degree. See color version of this figure at back of this issue.

ern latitudes warm less, in general, because of reduced convective overturning, which would normally bring warm water to the surface from the abyss [*Bryan and Spelman*, 1985; *Manabe et al.*, 1991]. The reduction of this supply of warm water leads to a reduced warming in most AOGCMs [*Cubasch et al.*, 2001]. Nevertheless, as Figure 5h shows, the maximum wintertime extent of sea ice retreats in both hemispheres.

[31] The salinity response to climate warming (Figure 5b) reflects the overall enhancement of the atmospheric hydrologic cycle that occurs due to the increased moisture-bearing capacity of warmer air [*Manabe et al.*, 1991]. The subtropical regions of high evaporation and salinity generally become saltier, whereas the higher-latitude regions of greater rainfall become fresher. The tropics also tend to become fresher, though not in the GFDL model.

[32] The combined effect of the temperature and salinity changes is an overall reduction of the surface density (Figure 5c). One would expect this reduced surface density to lead to increased vertical stratification (and thus to reduced nutrient supply). The vertical density gradient shown in Figure 5e supports this interpretation, with the exception of one AOGCM in each hemisphere (NCAR in the Northern Hemisphere and HADLEY in the Southern Hemisphere) over relatively small latitude bands. The impact of increased stratification is also reflected in the maximum mixed layer depth (MML in meters, Figure 5f), which is reduced in most AOGCMs, particularly in the CSIRO and GFDL simulations. The wide differences in MML responses between the models are related to the magnitude of the MML in the control simulations, which is much deeper in the CSIRO and GFDL simulations than any of the other AOGCMs. Poleward of 40°N, all the models except MPI show a decrease in MML. We also show in Figure 5g the change in the growing season length (GSL in days), which is related to the mixed layer depth and responds in the same way.

[33] Finally, Figure 5d shows the response of upwelling to climate warming. There is no clearly discernable pattern to this response except within a couple of degrees of the equator, where all the AOGCMs except MPI show a reduction. Overall, the equatorial and coastal upwelling within 15° of the equator drops by 6% (range of 2% to 15%) in the six AOGCMs.

4.2. Biogeographical Provinces

[34] Table 6 shows the mean over the AOGCMs of the areas of each biogeographical province and how these are affected by global warming, and Figure 6 shows the area changes for each model individually. The basic pattern of the global warming response is a contraction of the high surface chlorophyll marginal sea ice and seasonally mixed subtropical gyre biomes, which is only partly counterbalanced by an expansion of the high-chlorophyll subpolar gyre biome. The remaining available area, which is quite large in the Southern Hemisphere, goes primarily to the low-chlorophyll permanently stratified subtropical gyre biome. The marginal sea ice biome decreases globally by 42% in the Northern Hemisphere and 17% in the Southern Hemisphere by the middle of this century. The permanently stratified subtropical biome increases by 4.0% in the Northern Hemisphere and 9.4% in the Southern Hemisphere over the same time. Between these two regions, the subpolar gyre biome expands and the seasonally mixed subtropical biome contracts, with both shifting to higher latitudes and only a modest change in their combined area: an increase of 2.8% in the Northern Hemisphere, and a decrease of 2.0% in the Southern Hemisphere.

[35] The low-latitude upwelling biome also changes only modestly, increasing by 0.4% in the Northern Hemisphere, and decreasing by 2.5% in the Southern Hemisphere, and there is a shift of area from the downwelling provinces to

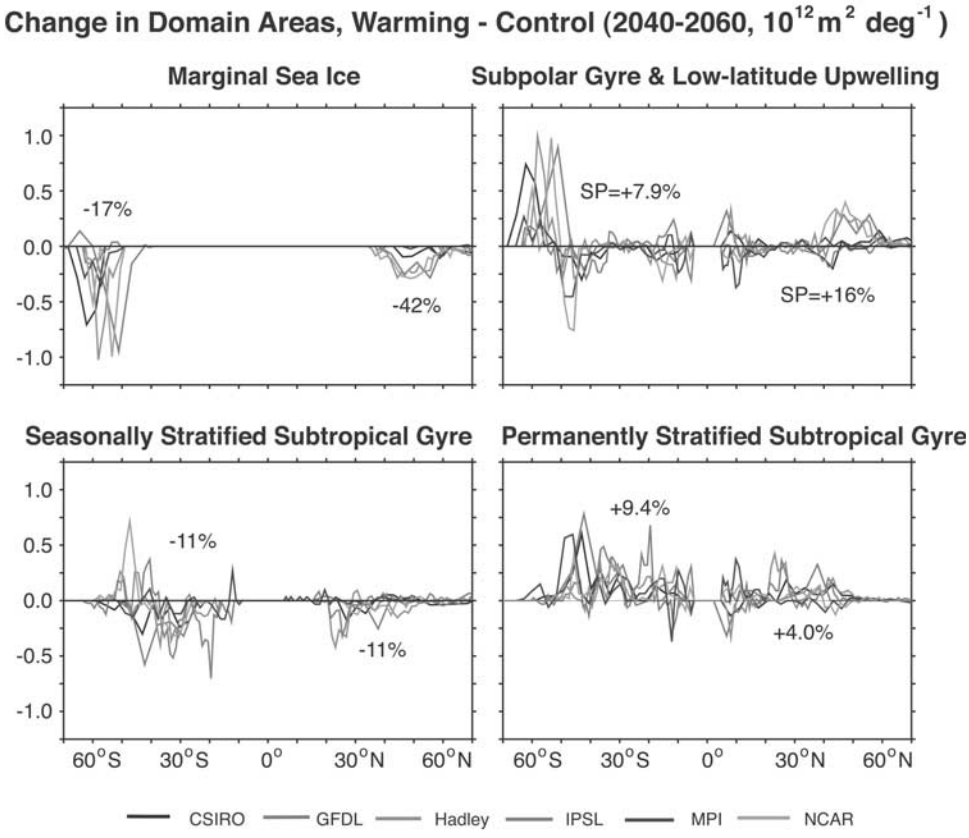

Figure 6. Zonally integrated changes in biome areas (warming minus control) for the six models. The units are 10^{12} m^2 per degree. Percent changes are also shown. The percent change for the combined subpolar gyre and low latitude upwelling biomes is just that due to the contribution of the subpolar gyre biome (SP). See color version of this figure at back of this issue.

the upwelling provinces in the equatorially influenced biome.

4.3. Chlorophyll

[36] Figure 7a shows the zonal geometric average of the annual mean SeaWiFS based chlorophyll, along with the zonal geometric average of chlorophyll predicted by the empirical model applied to each of the six control AOGCM simulations, with the AOGCM biomes shown in Figure 3. See the discussion above for how these biomes are further broken down into the 33 biogeographical provinces. The chlorophyll obtained using the control climate variables is generally in good agreement with the observed distribution. The relatively low values in the subtropics, particularly of the Northern Hemisphere, are consistent with the general difficulty of ocean general circulation models in obtaining sufficient nutrient supply into these regions [e.g., *Sarmiento et al.*, 1993]. The variables obtained from the models reflect the physical processes that are responsible for this reduced nutrient input. The low chlorophyll concentrations of the IPSL model between 50°N and 60°N occurs in the North Pacific, where the model-predicted mixed layer is too deep [*Bopp et al.*, 2001]. Similarly, the extraordinarily deep mixed layers in the GFDL model south of 50°S (>1000 m) result in low chlorophyll in this region of that model. Figure 7b shows primary production calculated with the chlorophyll from Figure 7a using the *Behrenfeld and Falkowski* [1997] primary production algorithm. The difference from model to model corresponds to that seen in the chlorophyll in Figure 7a.

[37] We now use the empirical model defined by equation (2) to calculate chlorophyll from the global warming simulation variables and subtract these from the control chlorophyll calculation in order to predict how the chlorophyll might respond to global warming. Figure 8 shows how chlorophyll predicted by the empirical model responds to global warming in the six AOGCMs. The quantity shown is

$$\Delta\mathrm{CHL} = \mathrm{CHL}_{\mathrm{warm}} - \mathrm{CHL}_{\mathrm{control}}, \qquad (3)$$

where the chlorophyll concentrations are calculated off-line with the empirical model (2) using the AOGCM diagnostics of SST, SSS, MML, and GSL. The primary features of Figure 8 on which most of the ΔCHL calculations are in agreement are (1) the drop in chlorophyll in the North Pacific in all of the estimates except those obtained with the IPSL and MPI diagnostics, (2) the increase in chlorophyll in the North Atlantic in all estimates except for some regions of those obtained with the HADLEY and NCAR diagnostics, (3) an increase in chlorophyll in all three basins of the Southern Ocean, albeit with patterns that differ from model to model, and (4) regions of decreased chlorophyll adjacent

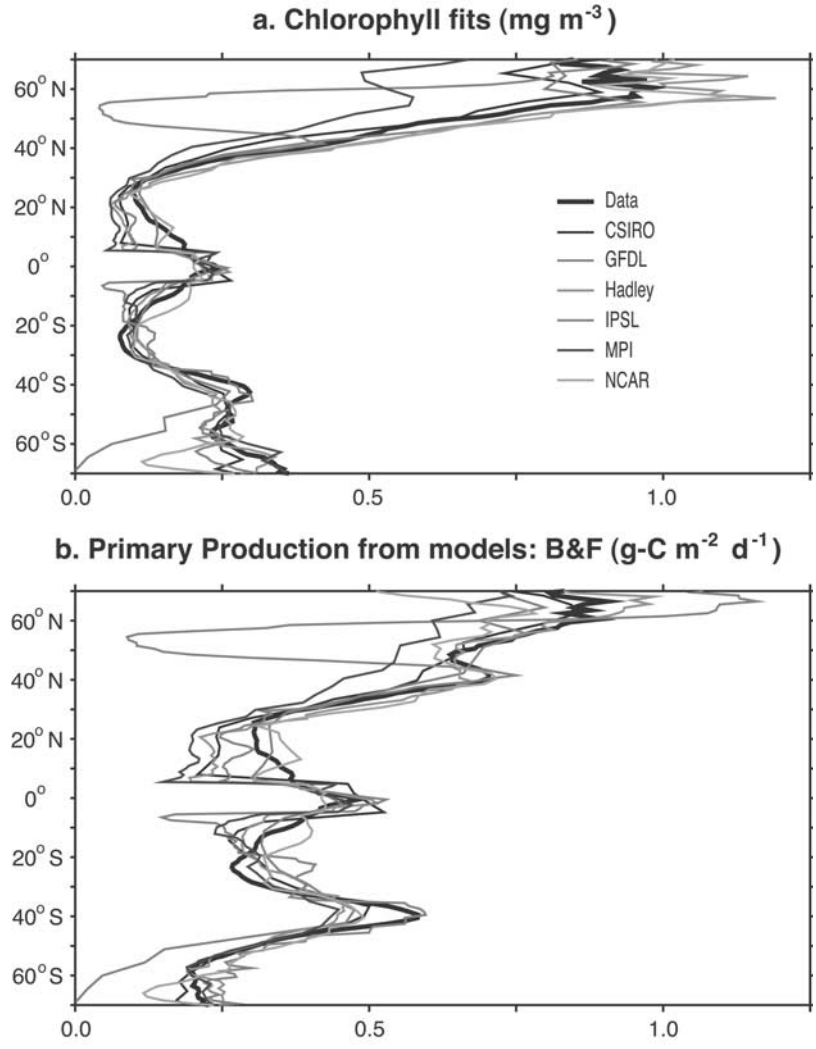

Figure 7. Zonal means of chlorophyll and primary production. (a) Chlorophyll in mg m^{-3} estimated using SeaWiFS color observations (thick black line) and chlorophyll estimated from AOGCM variables using the empirical model described in the text (thin lines). The model labels correspond to those given in Table 1. (b) Primary production in g m^{-2} d^{-1} of carbon derived from the SeaWiFS chlorophyll using the *Behrenfeld and Falkowski* [1997] algorithm. The line colors correspond to those in Figure 7a. See color version of this figure at back of this issue.

to the Antarctic in all estimates except those obtained using the GFDL diagnostics. There are a few additional features of interest in the chlorophyll distributions, such as off southwestern Africa. However, none of these carries across over more than one or two model simulations.

[38] The focus of the discussion below is to identify what causes the chlorophyll changes in the four regions identified above. We emphasize primarily the results obtained using the CSIRO, GFDL, HADLEY, and NCAR diagnostics. The biogeographical boundaries are very noisy in IPSL and thus difficult to interpret (this model is the primary reason that the North Pacific biome means shown in Table 8 do not agree with the impression one gets from Figure 8 of a decrease in chlorophyll), and the separation between the seasonally mixed and permanently stratified subtropical gyre biomes does not work very well in the MPI model because of the different way that the mixed layer is calculated in this model. We show in Figure 9a the chlorophyll change in regions where the biogeographical province boundaries shift between the warming and control scenarios. In regions where the biogeographical boundaries do not shift, we estimate the contribution of each variable in equation (2) using the approximate relationship

$$\begin{aligned}\Delta\mathrm{CHL} &\approx \sum_{i=1}^{4} \frac{\partial \mathrm{CHL}_{\mathrm{control}}}{\partial V_i} \times \Delta V_i, \\ &= \sum_{i=1}^{4} \mathrm{CHL}_{\mathrm{control}} \times \frac{\partial \ln(\mathrm{CHL}_{\mathrm{control}})}{\partial V_i} \times \Delta V_i, \\ &= \mathrm{CHL}_{\mathrm{control}} \times \sum_{i=1}^{4} a_i \times \Delta V_i, \end{aligned} \tag{4}$$

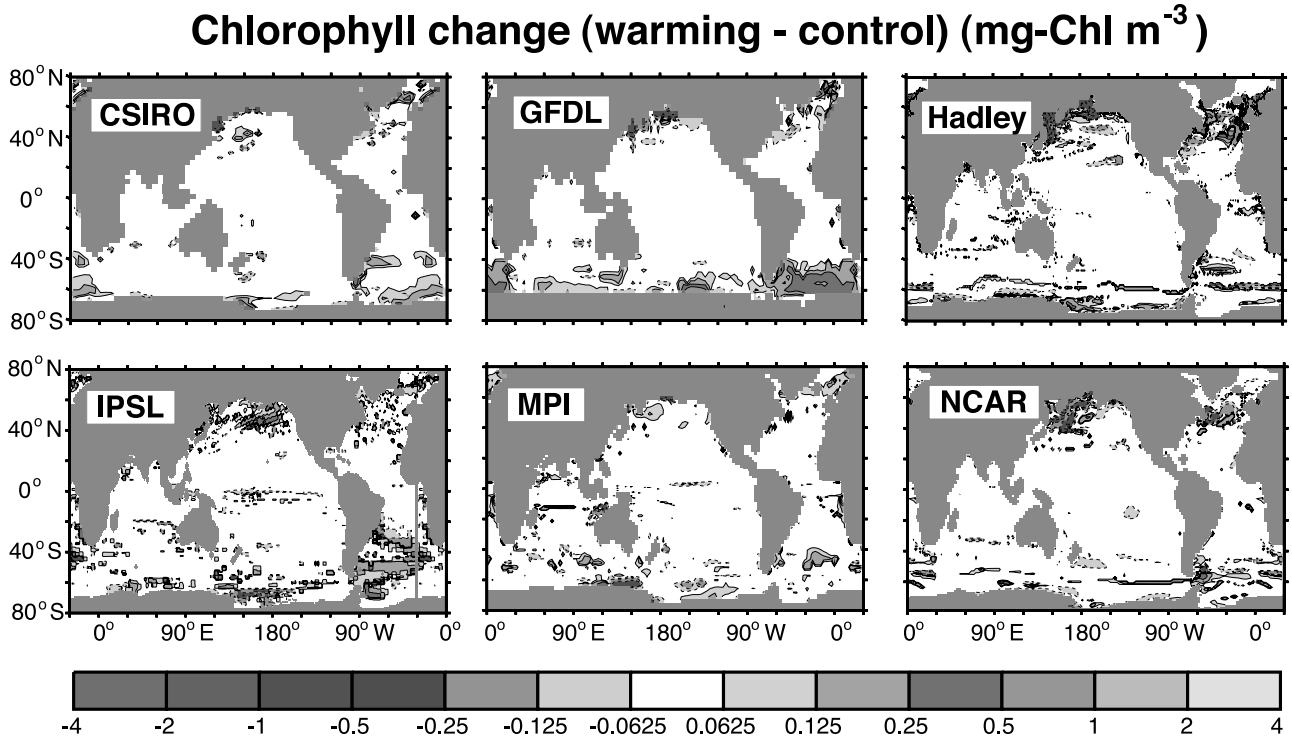

Figure 8. Impact of the global warming simulations on the chlorophyll concentration in mg m^{-3}. Chlorophyll is calculated for both the control and the warming simulations using the empirical model (equation (2)). The figure shows the difference between the warming simulation and the control simulation averaged over the period 2040 to 2060 (except for MPI, which is for the period 2040 to 2049). Areas in white are those for which the chlorophyll change is smaller than ±0.0625 mg m^{-3}. See color version of this figure at back of this issue.

where V_i and a_i are the variables and parameters defined by equations (2). Figure 9b shows the chlorophyll change due to the combined contribution of the SST′ and SSS′ terms, which we have referred to as water mass tracers. Our definition of the water mass tracers requires that the average of these over a given province should be equal to 0, and therefore that their province wide average contribution to ln(CHL) should be equal to 0. However, we consider here the behavior of CHL, not ln(CHL), for which this constraint does not apply. This explains why one does not generally

Table 8. Average Response of Chlorophyll Concentrations (mg m^{-3}) to Global Warming for the Period 2040 to 2060[a]

	Indian Ocean			Pacific Ocean			Atlantic Ocean			Global		
	Control	Δ	%Δ	Control	Δ	%Δ	Control	Δ	%Δ	Control	Δ	%Δ
Northern Hemisphere												
Marginal sea ice				1.08	0.012	1.1	0.99	−0.009	−0.9	1.02	−0.011	−1.1
Subpolar				0.37	0.048	12.8	0.69	0.019	2.8	0.46	0.051	11.1
Subtropical seasonal				0.27	0.007	2.6	0.31	0.022	7.0	0.30	0.021	7.0
Subtropical permanent	0.30	0.005	1.7	0.10	0.006	6.2	0.13	0.002	1.6	0.11	0.006	5.5
Low-latitude upwelling	0.22	0.013	6.0	0.09	0.007	8.2	0.21	0.005	2.4	0.12	0.006	5.0
5°S to 5°N												
Upwelling	0.19	−0.004	−2.1	0.23	−0.010	−4.4	0.29	0.005	1.7	0.23	−0.006	−2.6
Downwelling	0.18	0.003	1.6	0.21	−0.003	−1.4	0.24	0.000	0.0	0.20	−0.001	−0.5
Southern Hemisphere												
Low-latitude upwelling	0.11	0.001	0.9	0.10	0.002	2.0	0.49	0.002	0.4	0.14	0.008	5.8
Subtropical permanent	0.12	0.001	0.8	0.11	0.000	0.0	0.15	0.004	2.6	0.12	0.001	0.8
Subtropical seasonal	0.24	0.003	1.2	0.15	0.003	2.1	0.26	0.004	1.6	0.20	0.006	3.0
Subpolar	0.23	0.006	2.6	0.22	0.008	3.6	0.32	0.083	25.9	0.24	0.022	9.1
Marginal sea ice	0.20	0.011	5.4	0.26	0.047	17.8	0.21	0.094	45.2	0.22	0.051	23.5

[a]Δ is warming minus control. Chlorophyll concentrations are obtained using the empirical model (equation (2)) with variables obtained from each AOGCM (except MPI), and then the geometric mean is calculated over each biogeographical province. The table shows the mean response of the chlorophyll estimated from the five AOGCMs simulations. In cases where a particular model is missing from either the control or warming scenario (see Table 6 footnote), that model is excluded for both the control and Δ averages for that specific basin, but not for the global mean.

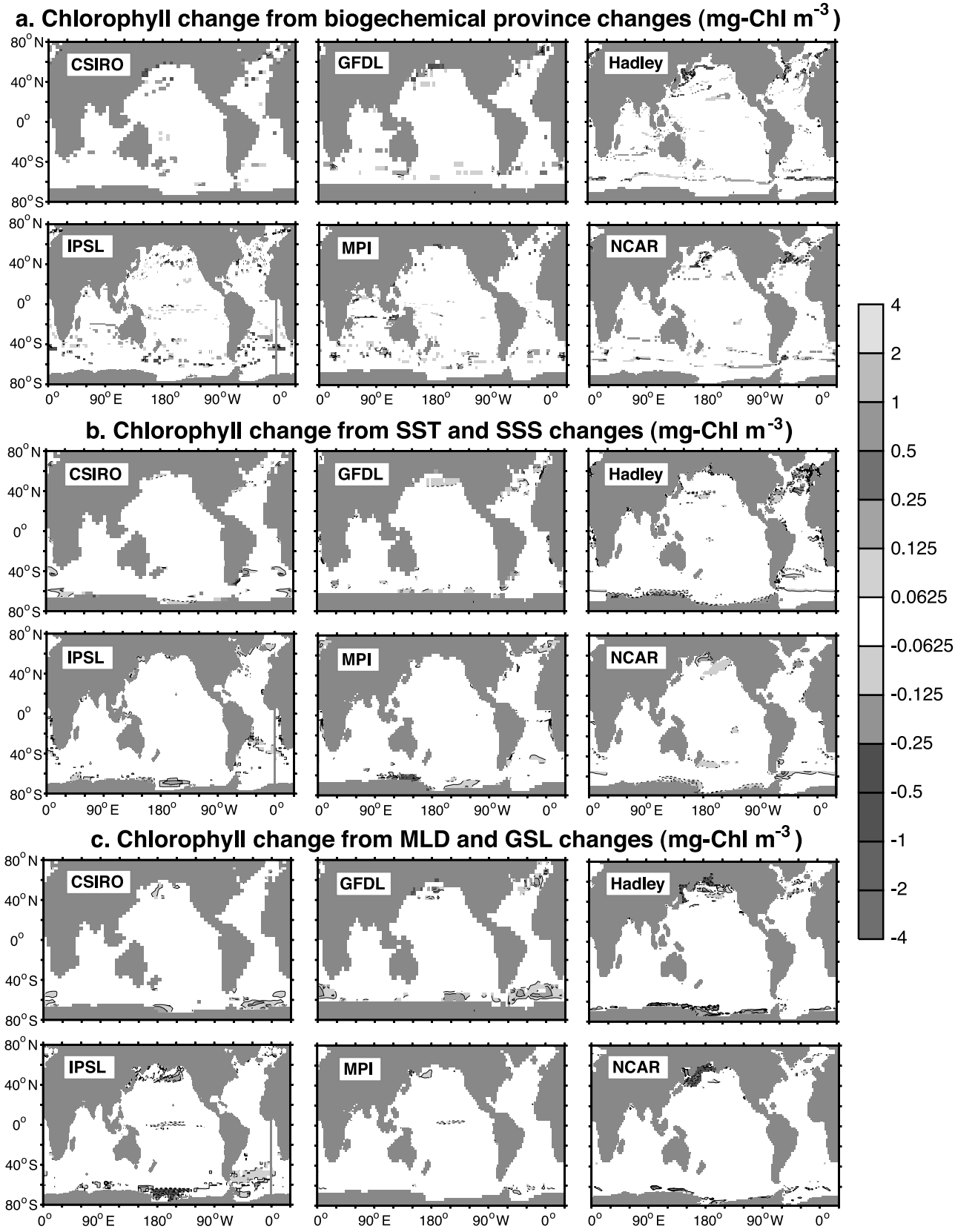
a. Chlorophyll change from biogechemical province changes (mg-Chl m-3)
b. Chlorophyll change from SST and SSS changes (mg-Chl m-3)
c. Chlorophyll change from MLD and GSL changes (mg-Chl m-3)
CSIRO
GFDL
Hadley
IPSL
MPI
NCAR
80°N
40°N
0°
40°S
80°S
0°
90°E
180°
90°W
4
2
1
0.5
0.25
0.125
0.0625
-0.0625
-0.125
-0.25
-0.5
-1
-2
-4

Figure 9

see regions of negative chlorophyll change balancing regions of positive chlorophyll change in Figure 9b. Figure 9c shows the contribution of the MML and GSL terms, the first of which is a measure of nutrient supply, and the second a measure of the light supply.

4.3.1. North Pacific

[39] The decrease in chlorophyll in this region is due primarily to replacement of the marginal sea ice biome by the less productive subpolar biome (Figure 9a). Increases in the growing season length also contribute to the chlorophyll reduction calculated from the HADLEY and NCAR diagnostics (Figure 9c). This is the opposite of what one might expect, and suggests perhaps that growing season length is parameterizing nutrient supply rather than light supply, with a longer period signifying less supply by deep wintertime mixing.

4.3.2. North Atlantic

[40] The North Atlantic is a region where many different biomes are packed close to each other in a small region. The response of the chlorophyll in this region is accordingly complex, reflecting a combination of province boundary changes as well as water mass property and transport tracer changes, with regions of negative as well as positive chlorophyll response. It is difficult to discern any characteristic response pattern.

4.3.3. Southern Ocean

[41] The most important region in determining the Southern Ocean chlorophyll increase in most of the ΔCHL calculations is the marginal sea ice biome. The retreat of this biome gives rise to the chlorophyll increase in the Indian and Pacific Oceans that can be seen as a linear feature at about 60°S (Figure 9a). This increase is perhaps a bit surprising in that the average marginal sea ice biome chlorophyll is higher than the subpolar biome (Table 5). However, the specific region that shifts from one biome to another has lower chlorophyll in the control simulation than in the climate warming simulation. The linear feature is particularly noticeable in chlorophyll calculated with the GFDL, HADLEY, and NCAR diagnostics. A similar linear feature but of opposite sign is seen in the Atlantic Ocean of the HADLEY and NCAR models, due again to the retreat of the marginal sea ice zone.

[42] Within the marginal sea ice biome, there are large areas of increased chlorophyll that are particularly notable in ΔCHL calculated using the CSIRO and GFDL diagnostics, but also closer to the continent in the HADLEY and NCAR calculations (Figure 8). These are all due to reductions in the mixed layer depth (compare Figure 9c), which are particularly large in the CSIRO and GFDL models. The IPSL model has a large increase in the southern Atlantic Ocean that is also due to shallowing of the mixed layer, but in the seasonally mixed subtropical gyre biome.

4.3.4. Southern Ocean Adjacent to Antarctica

[43] Adjacent to the continents there are some very small regions of reduced chlorophyll concentration in all the models. These are all due to changes in SSS′ (compare Figure 9b), except for ΔCHL calculated from the IPSL diagnostics, which has a large region of reduced chlorophyll due to changes in MML in the marginal sea ice biome (Figure 9c). Analysis of the SSS response to warming (Figure 5b) shows a tendency for the freshening of surface waters to be greater as the continent is approached in most of the models, which is the main cause of the chlorophyll change predicted by the empirical model.

[44] The climate responses we infer from Figure 8 are often inconsistent with the province means shown in Table 8. The province means in Table 8 show a consistent pattern of increase outside the equatorially influenced biome, and a decrease within the equatorially influenced biome. Some of the increases are quite large, for example in the Southern Hemisphere marginal sea ice biome and Southern and Northern Hemisphere subpolar biomes. This inconsistency reflects the dominance of a few model results (such as, for example, IPSL in the North Pacific) in the averages.

4.4 Primary Production

[45] Figure 10 shows the zonal mean response of primary production to warming in the six AOGCM simulations using the *Behrenfeld and Falkowski* [1997] (hereinafter B&F) primary production algorithm, with chlorophyll given by the empirical model (2). Figure 11 compares the mean response of primary production using the B&F function with those of *Carr* [2002], and *Marra et al.* [2003] (hereinafter CARR and MARRA, respectively). The quantity shown is

$$\Delta PP = PP_{warm} - PP_{control}. \quad (5)$$

Both figures show the total response (Figures 10c and 11c) as well as the response to the chlorophyll change alone (Figures 10a and 11a) and to the temperature change alone (Figures 10b and 11b). Table 9 summarizes the mean in situ primary production for each biogeographical province, and Table 10 summarizes the area integral over each biogeographical province. Only the B&F and MARRA results are shown in the tables, as in combination these always

Figure 9. Impact of the global warming simulations on the chlorophyll concentration in mg m^{-3} as in Figure 8, but broken down into various components. The global ocean is first separated into regions where the biogeographical provinces changed from one to another (e.g., marginal ice biome to subpolar biome) and regions where it did not. (a) Contribution to the total chlorophyll response that occurs in regions where the biogeographical provinces changed. (b, c) Changes in regions where the biogeographical provinces remained the same. Figure 9b shows the contribution to the total chlorophyll response that is due to changes in water mass properties: sea surface temperature anomaly (SST′) and sea surface salinity anomaly (SSS′) calculated using equation (4). Figure 9c shows the contribution to the total chlorophyll response that is due to the combined influence of changes in the maximum wintertime mixed layer depth (MLD) and the growing season length (GSL), again calculated using equation (4). The sum of Figures 9a, 9b, and 9c is approximately but not exactly equal to Figure 8 because of the nonlinearity of the chlorophyll empirical equation, which means that the breakdown given by equation (4) is not exact. See color version of this figure at back of this issue.

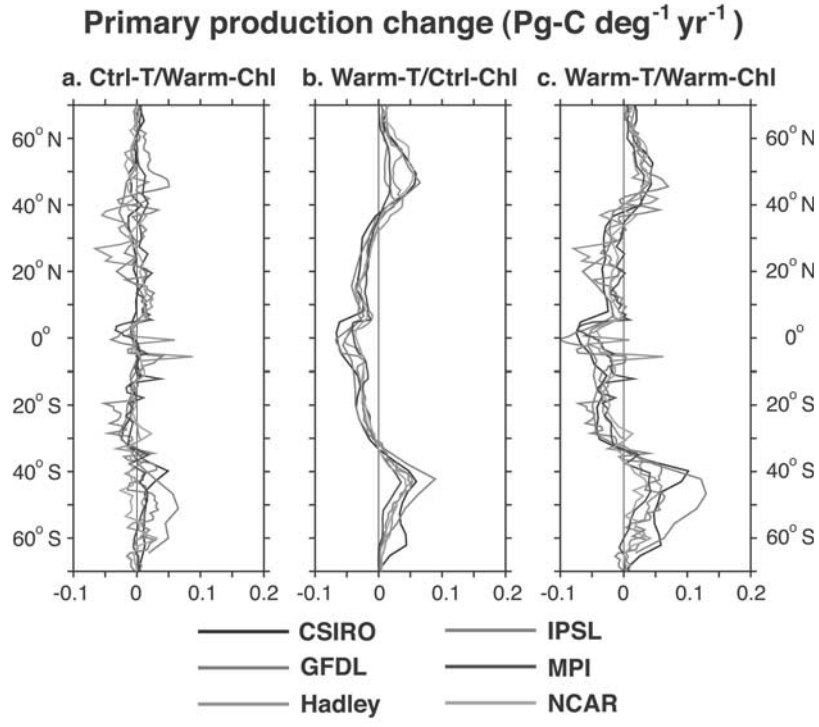

Figure 10. Zonally integrated response of primary production calculated with the *Behrenfeld and Falkowski* [1997] algorithm using chlorophyll calculated from the empirical model (equation (2)). The figure shows the difference between the warming and the control simulation for each of the six AOGCMs averaged over the period 2040 to 2060 (except for MPI, which is for the period 2040 to 2049). (a) The increase in primary production that occurs in response to the chlorophyll change only, with temperature kept constant at the control scenario. (b) The increase in primary production that occurs in response to the temperature increase only, with chlorophyll kept constant at the control scenario. (c) The increase in primary production that occurs in response to the combined effect of the chlorophyll change and temperature increase. See color version of this figure at back of this issue.

represent the upper and lower limits of the warming response (compare Figures 10 and 11).

[46] The salient results of the primary production estimates are (1) the high sensitivity of the chlorophyll dependence to the AOGCM (Figure 10a), but relatively low sensitivity to the primary production algorithm (Figure 11a), and (2) the relatively low sensitivity of the temperature dependence to the climate model (Figure 10b), but high sensitivity to the primary production algorithm (Figure 11b). As regards the sensitivity to chlorophyll (Figure 11a), the B&F and MARRA primary production algorithms give virtually identical results. Only the CARR algorithm differs from the others, showing greater sensitivity of primary production to the chlorophyll changes in the tropics. We note that the chlorophyll contribution to the primary production change is generally quite small and rather noisy (Figure 10a). In those few regions where there is a strong response, such as in the Southern Ocean in the GFDL model, and in the tropics at ~8°S in the HADLEY and IPSL models, the signals are due to at most two models, which does not give us great confidence in their robustness. Note that the Southern Ocean and 8°S chlorophyll responses, as well as other large chlorophyll-driven responses at other latitudes, carry over quite strongly into the model means shown in Figure 11a. However, as Figure 10a clearly indicates, in every case, these larger signals are due to the influence of just one or two models.

[47] The main features of the temperature response of the primary production are (1) the B&F algorithm shows a large decrease in the tropics where the CARR and MARRA algorithms show an increase, (2) the MARRA algorithm shows a greater sensitivity to the temperature increase in the tropics than the CARR algorithm, and (3) the B&F algorithm shows the greatest sensitivity to warming in the high latitudes, followed by the CARR algorithm, with the MARRA algorithm showing almost no change in high-latitude primary production. All of these features can be understood by reference to the analysis in Figure 4a, and are directly related to the magnitude of the control climate primary productions shown in Figure 4b. Note that the change from 2050 to 2090 is quite small in the tropics except for the MARRA algorithm, and also in the high latitudes except for the B&F algorithm (Figures 11b and 11c). As noted earlier, the few places where there are larger responses, such as at 8°S, are due to one or two models only.

[48] The percent changes in the mean primary production of the different provinces summarized in Table 9 show many quite large effects, such as the increases in the marginal sea ice and subpolar biomes in both the Northern and Southern Hemispheres. As one moves equatorward into

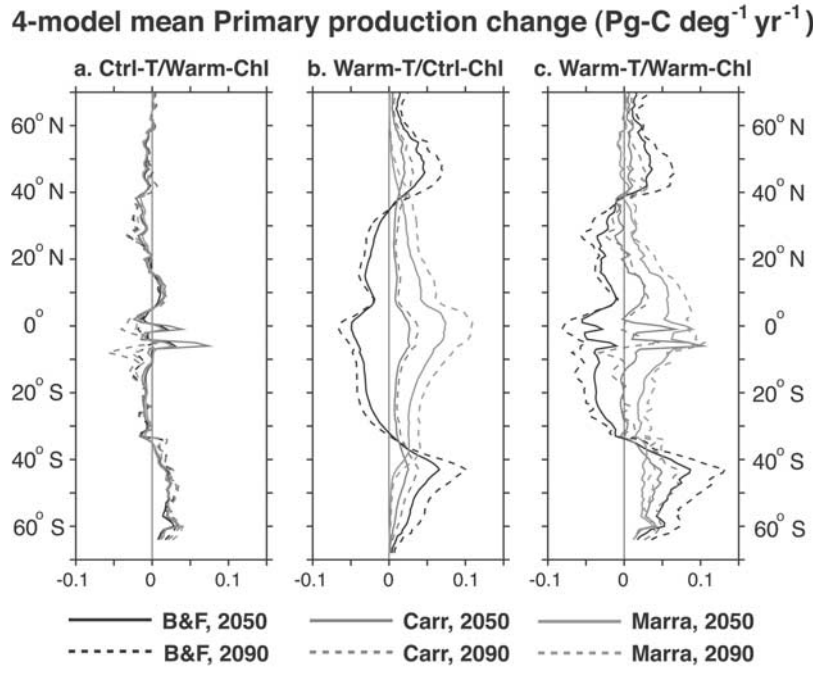

Figure 11. The mean over the CSIRO, GFDL, Hadley, and NCAR models of the response of zonally integrated primary production to global warming. The MPI and IPSL models are excluded, the former because the simulation ended in 2049, the latter because of the difficulties encountered in defining the biome boundaries; compare Figure 3. The primary production responses are calculated as in Figure 10 (warming minus control), but with the three different primary production algorithms of *Behrenfeld and Falkowski* [1997] (B&F), *Carr* [2002] (Carr), and *Marra et al.* [2003] (Marra). The figure shows both the average over the period 2040 to 2060 (labeled 2050) and the average over the period 2080 to 2100 (labeled 2090). The three panels are calculated as described in the Figure 10 caption. See color version of this figure at back of this issue.

the seasonally mixed subtropical gyre biome, one sees that the B&F algorithm gives a smaller response than the MARRA algorithm, with a change in sign of the B&F algorithm occurring finally in the subtropical permanent, low-latitude upwelling, and equatorially influenced biomes.

[49] The integrated primary production results summarized in Table 10 represent the combined effect of the primary production changes of Table 9 with the area changes of Table 6. The large reduction in area of the Northern Hemisphere subpolar gyre marginal sea ice biome overwhelms the increase in average primary production in this region, resulting in a net reduction of 33% and 39% in the total primary production calculated with the B&F and MARRA algorithms, respectively. By contrast, a large increase occurs in the Northern Hemisphere subpolar gyre biome, where the changes in area and average primary production have the same sign. Total primary production in the Southern Hemisphere subpolar biome also increases by a large amount for the same reason, but the marginal sea ice biome in this hemisphere changes only modestly due to a cancellation between the large increase in primary production and smaller area decrease in this hemisphere than in the Northern Hemisphere.

[50] The remaining lower latitude biomes are the ones where average primary production decreases with the B&F algorithm, but increases with the MARRA algorithm. Thus MARRA shows a large increase in the permanently stratified subtropical gyre due to increases in both the average primary production and area, where B&F shows a more modest increase due to the fact that average primary production decreases, and the B&F algorithm gives a decrease in the low-latitude upwelling and equatorially influenced biomes, where MARRA shows an increase. The disagreement is quite large. Overall, if we use B&F for the marginal sea ice and subpolar gyre biomes, and MARRA for the lower latitude biomes, the global primary production in the control climate is 44.3 Pg C yr^{-1}, and the increase is 4.2 Pg C yr^{-1}, i.e., 9.6%. If instead we use MARRA for the high latitudes, and B&F for the low latitudes, the global primary production in the control climate drops to 42.3 Pg C yr^{-1} and the global warming simulation leads to a decrease of 0.5 Pg C yr^{-1}, i.e., −1.3%.

5. Discussion and Conclusions

[51] The first point we would make is that model comparison studies such as this are hard to craft and the results are not easy to interpret. The summaries of the models in Table 2, and the diagnostics and information given in Tables 3 and 4, capture only some of the myriad ways in which these models differ from each other. The variations include that some models use flux adjustments to prevent

Table 9. Predicted Response of Primary Production (mg carbon m^{-2} d^{-1}) to Global Warming for the Period 2040 to 2060[a]

	Indian Ocean			Pacific Ocean			Atlantic Ocean			Global		
	Control	Δ	%Δ	Control	Δ	%Δ	Control	Δ	%Δ	Control	Δ	%Δ
B&F Model												
Northern Hemisphere												
Marginal sea ice				667	99	14.9	655	80	12.2	650	85	13.2
Subpolar				477	97	20.5	934	46	4.9	609	101	16.5
Subtropical seasonal				579	9	1.6	647	26	4.0	626	25	3.9
Subtropical permanent	528	−34	−6.4	282	−3	−1.1	352	−25	−7.2	309	−9	−2.9
Low-latitude upwelling	417	−16	−3.9	222	−4	−1.7	448	−38	−8.5	286	−11	−4.0
5°S to 5°N												
Upwelling	375	−23	−6.0	477	−58	−12.2	540	−50	−9.3	465	−49	−10.5
Downwelling	355	−9	−2.5	413	−26	−6.4	468	−47	−10.0	395	−21	−5.4
Southern Hemisphere												
Low-latitude upwelling	280	−18	−6.6	254	−9	−3.4	873	−73	−8.4	326	−9	−2.8
Subtropical permanent	334	−15	−4.5	327	−14	−4.2	406	−7	−1.7	343	−12	−3.4
Subtropical seasonal	523	23	4.3	340	16	4.8	547	16	3.0	444	25	5.7
Subpolar	283	17	5.9	317	21	6.7	356	88	24.6	314	33	10.6
Marginal sea ice	158	28	17.9	233	29	12.6	159	58	36.3	179	40	22.2
MARRA Model												
Northern Hemisphere												
Marginal sea ice				664	28	4.2	641	13	2.0	648	13	2.0
Subpolar				322	35	10.7	556	18	3.2	397	35	8.9
Subtropical seasonal				361	24	6.5	392	40	10.2	384	38	10.0
Subtropical permanent	805	84	10.4	270	34	12.5	351	26	7.5	307	35	11.3
Low-latitude upwelling	624	81	12.9	330	49	14.8	585	67	11.4	412	54	13.2
5°S to 5°N												
Upwelling	615	49	8.0	663	44	6.6	777	83	10.6	671	52	7.8
Downwelling	591	69	11.7	669	55	8.2	676	55	8.2	636	63	10.0
Southern Hemisphere												
Low-latitude upwelling	391	39	9.9	344	34	9.9	947	72	7.6	437	51	11.6
Subtropical permanent	299	24	8.1	273	12	4.5	307	14	4.4	282	17	6.1
Subtropical seasonal	292	9	3.0	193	6	3.0	332	22	6.5	253	12	4.7
Subpolar	192	2	1.1	189	6	2.9	263	52	19.8	204	13	6.4
Marginal sea ice	169	12	6.9	213	31	14.7	196	59	30.2	190	34	17.7

[a]Primary production is calculated using two of the primary production models (B&F is from *Behrenfeld and Falkowski* [1997], and MARRA is from *Marra et al.* [2003]) with chlorophyll calculated from the AOGCM results (except for MPI) using the empirical model (equation (2)). The geometric mean for each province in each model is obtained first, and then all five models are averaged together for each province. See Table 8 footnote regarding models that were excluded in calculating the primary production averages.

climate drift whereas others do not, that both horizontal and vertical model resolutions differ by almost a factor of 4, and that the sub-grid mixing parameterizations vary considerably. Because of the differences in vertical resolutions of the models (or, in the case of the MPI model, the depth to which this particular diagnostic was interpolated and then saved when the model was run), the depths at which the diagnostics were obtained for upwelling into the surface layer and vertical density gradient at the base of the surface layer ranged from 24.45 m to 100 m (Table 4). The mixed layer depth was problematic in part because one of the models, MPI, uses an ocean component formulated on isopycnic coordinates [*Oberhuber*, 1993]. In that model the mixed layer depth is a prognostic model variable, whereas in the other models a density criterion is used to determine the mixed layer depth a posteriori. In addition, the fundamental physics differs significantly from model to model, for example, in how to deal with vertical instability, which some models respond to by convecting and others by enhancing vertical mixing. We would like to be able to provide explanations for the differences in responses of variables such as those shown in Figure 5 in terms of the basic physics of the models, but our ability to do so is governed almost entirely by our initial choice of diagnostics, which was quite limited in this study.

[52] Another problem is with biases in the control climate simulations. The biome boundaries defined from the control climate simulations provide a good illustration of this problem, with large differences between one model simulation and another (Figure 3), and between these and the boundaries defined from observations (Figure 2b). A particular difficulty is with the marginal sea ice zone biome, which covers an average area of 11% in the models versus 6.0% in the observations. Most of the excess area in the models comes from the permanently stratified subtropical gyre biome, which covers only 38% in the model average, versus 45% in the observations.

[53] We have an additional problem in our study in that we are dealing not only with uncertainties in the physical response of the climate, but also with deep uncertainties in our understanding of biology and how it will respond to climate change. Our empirical modeling approach for predicting chlorophyll allows us to easily compare large numbers of AOGCMs with each other, but it implicitly assumes that the spatial relationships between biomass and physical forcing that we find from observations in the present ocean imply a mechanistic connection that can be applied to temporal changes into the future. This assumption can only be tested to a very limited extent without long-term global observations, which are only now starting to become available.

Table 10. Predicted Response of Integrated Primary Production (Pg carbon yr^{-1}) to Global Warming for the Period 2040 to 2060[a]

	Indian Ocean			Pacific Ocean			Atlantic Ocean			Global		
	Control	Δ	%Δ	Control	Δ	%Δ	Control	Δ	%Δ	Control	Δ	%Δ
B&F Model												
Northern Hemisphere												
Marginal sea ice				1.29	−0.47	−36.2	0.82	−0.24	−29.6	1.85	−0.61	−33.2
Subpolar				1.61	0.60	37.4	1.89	0.43	22.7	3.51	1.03	29.4
Subtropical seasonal				1.07	−0.14	−13.1	2.08	−0.09	−4.4	3.15	−0.23	−7.4
Subtropical permanent	0.69	−0.04	−5.1	3.84	0.16	4.1	1.64	0.01	0.6	6.16	0.13	2.2
Low-latitude upwelling	0.36	−0.04	−11.1	0.97	−0.02	−2.3	0.78	−0.06	−7.9	2.11	−0.12	−5.8
5°S to 5°N												
Upwelling	0.62	0.02	2.6	2.74	−0.33	−11.9	0.97	−0.08	−7.8	4.34	−0.39	−8.9
Downwelling	0.30	−0.07	−22.3	0.85	−0.10	−11.6	0.25	−0.02	−9.3	1.18	−0.17	−14.0
Southern Hemisphere												
Low-latitude upwelling	0.84	−0.06	−7.4	0.96	−0.10	−10.2	1.37	−0.01	−0.9	3.18	−0.17	−5.4
Subtropical permanent	1.85	0.06	3.4	4.50	0.25	5.4	2.18	0.32	14.7	8.53	0.63	7.4
Subtropical seasonal	2.71	0.00	0.1	1.48	−0.16	−11.0	1.62	−0.20	−12.0	5.49	−0.32	−5.8
Subpolar	0.91	0.24	26.0	1.57	0.13	8.4	1.10	0.22	19.5	3.58	0.59	16.4
Marginal sea ice	0.53	−0.04	−8.1	0.78	−0.05	−6.3	0.61	0.04	6.9	1.91	−0.05	−2.7
GRLobal	8.82	0.07	0.8	21.67	−0.22	−1.0	15.30	0.32	2.1	44.98	0.32	0.7
MARRA Model												
Northern Hemisphere												
Marginal sea ice				1.31	−0.54	−41.0	0.74	−0.26	−35.6	1.79	−0.69	−38.9
Subpolar				1.00	0.31	30.5	1.15	0.26	22.2	2.15	0.56	26.1
Subtropical seasonal				0.69	−0.06	−8.5	1.26	−0.01	−0.6	1.95	−0.07	−3.5
Subtropical permanent	1.02	0.13	12.5	3.64	0.59	16.3	1.69	0.25	15.0	6.35	0.97	15.3
Low-latitude upwelling	0.52	0.03	5.4	1.36	0.21	15.7	0.99	0.11	11.1	2.87	0.35	12.3
5°S to 5°N												
Upwelling	1.01	0.19	18.3	3.63	0.32	8.7	1.37	0.17	12.7	6.02	0.67	11.2
Downwelling	0.50	−0.06	−11.3	1.32	0.06	4.5	0.35	0.00	1.1	1.84	−0.01	−0.3
Southern Hemisphere												
Low-latitude upwelling	1.18	0.10	8.2	1.27	0.02	1.9	1.50	0.20	13.2	3.95	0.32	8.1
Subtropical permanent	1.73	0.30	17.6	4.02	0.63	15.7	1.56	0.30	18.9	7.31	1.23	16.8
Subtropical seasonal	1.55	−0.01	−0.5	0.85	−0.10	−11.3	1.00	−0.11	−11.0	3.20	−0.19	−6.0
Subpolar	0.59	0.13	21.3	0.90	0.06	6.5	0.78	0.13	16.2	2.27	0.31	13.6
Marginal sea ice	0.55	−0.09	−16.4	0.71	−0.03	−4.8	0.66	0.05	6.8	1.92	−0.08	−4.1
GRLobal	8.65	0.71	8.2	20.70	1.48	7.1	13.06	1.08	8.3	41.61	3.38	8.1

[a]Primary production is calculated for each model as discussed in Table 9, then integrated for each biogeographical province in each model, then averaged over all the AOGCMs except MPI.

[54] On the other hand, the problem of climate warming and how ocean biology will respond to it is a crucial one that we need to address even if our understanding is imperfect. There have already been a few studies using prognostic models to determine the response of ocean biology to warming [*Cox et al.*, 2000; *Bopp et al.*, 2001; *Boyd and Doney*, 2002]. As we noted earlier, we believe that the ecosystem models on which such studies are based are immature and that much work needs to be done before their results can be trusted. Furthermore, with only a few such models in existence, and given the large differences between coupled climate model simulations of climate warming, it is difficult to get a clear sense of how uncertain the predicted responses are.

[55] Perhaps the most robust result of our study is the changes in biome areas that occur in response to global warming (Figure 6). These include a large reduction in the marginal sea ice biome and increase in the permanently stratified subtropical gyre biome. Between these two biomes, the subpolar gyre biome expands, and the seasonally stratified subtropical gyre biome contracts, with the combined change of these two being relatively small. Perhaps the least robust result of our study is the chlorophyll response that we predict with our empirical model. This is mostly relatively small, with big disagreements between models except for the four major features we identified and discussed earlier in the text (the North Pacific reduction, the North Atlantic increase, the open Southern Ocean increase, and the decrease adjacent to the Antarctic continent). Finally, the primary production changes that we predict have a coherent meridional pattern of response in the zonal means, but with big differences between the various primary production algorithms that we employed. The differences between the algorithms are due almost entirely to the temperature sensitivity illustrated in Figure 4a. While we do not know which, if any, of the primary production algorithms is correct, the magnitude and robustness of the response clearly points toward the importance of getting this right.

[56] Our study leads us to three major conclusions regarding how we may gain a better understanding of the response of oceanic biology to climate warming in the future:

[57] 1. The most critical factor in determining the oceanic response of primary production to climate warming may be the temperature sensitivity of primary production for a given chlorophyll content. The striking differences in temperature sensitivity between the three primary production algorithms illustrated in Figure 4a lead to dramatic differences in the global warming responses, as illustrated in Figure 11b. At issue are such fundamental questions as whether warming

would lead to a decrease or increase of primary production in the low latitudes, and whether the effects of warming would lead to essentially no change or quite a large increase in high-latitude primary production.

[58] Which of these primary production algorithms is most representative of reality? While we acknowledge the pioneering nature of these early algorithms and the insights they afforded us, our results clearly indicate that it is time that we obtain additional measurements to determine which of the algorithms is more realistic, and that we clarify the theoretical underpinning of these analyses so that we clearly isolate nutrient effects such as those that are the probable cause of the reduction in the *Behrenfeld and Falkowski* [1997] algorithm at temperatures above 20°C, from direct temperature effects.

[59] We have not included estimates of export production in this study, which could be made using algorithms of the ratio of export to primary production such as that of *Laws et al.* [2000]. These algorithms depend on the primary production per se, but also introduce additional temperature dependence that would have a significant impact on how export production responds to climate change.

[60] 2. We believe that the biogeographical mapping and empirical chlorophyll modeling approaches that we employed here have the potential to contribute significantly to our understanding of what controls oceanic ecosystems and their productivity and how these will respond to global warming [cf. *Boyd and Doney*, 2002]. Our analysis of oceanic observations in this context, which builds on earlier efforts such as that of *Longhurst* [1994], will, we hope, be followed by further research on this subject, including such issues as taking seasonal information into account [e.g., *Platt and Sathyendranath*, 1999], and exploring more sophisticated methods for reformulating the available information into orthogonal non-overlapping functions. Despite the fact that most of us are involved in one way or another with the development of prognostic ecosystem models for prediction of biological response to climate change, we maintain a healthy skepticism of such models and strongly urge further work on empirical approaches such as those we used here. We believe that the large differences in chlorophyll response illustrated in Figures 8 and 9 are reflective of real uncertainties arising from differences in model physics that merit careful attention.

[61] 3. Finally, we emphasize that there are large differences between AOGCM simulations of warming that lead to large uncertainties in the predicted biological response. Model comparison studies such as this are difficult to carry out and their results hard to interpret, but they are essential to developing a realistic assessment of the future response of oceanic biology to climate warming.

[62] **Acknowledgments.** J. L. Sarmiento and R. Slater were supported by the NOAA Office of Global Programs grant NA56GP0439 to the Carbon Modeling Consortium for model development and by NSF grant OCE00973166 for model and observational interpretations as part of the JGOFS Synthesis and Modeling Project. R. Barber was supported by NSF grant OCE 0136270 as part of the JGOFS Synthesis and Modeling Project. S. Doney and J. Kleypas wish to thank the Community Climate System Model science team and the Climate Simulation Laboratory at NCAR and acknowledge support from NOAA-OGP grant NOAA-NA96GP0360S. Spall is funded through the UK Department for Environment, Food and Rural Affairs contract PECD 7/12/37.

References

Alexander, R. C., and R. L. Mobley (1976), Monthly average sea surface temperatures and ice pack limits on a 1° global grid, *Mon. Weather Rev.*, *104*, 143–148.

Aumont, O., J. C. Orr, P. Monfray, G. Madec, and E. Maier-Reimer (1999), Nutrient trapping in the equatorial Pacific: The ocean circulation solution, *Global Biogeochem. Cycles*, *13*(2), 351–369.

Barber, R. T. (1992), Geologic and climatic time scales of nutrient variability, in *Primary Productivity and Biogeochemical Cycles in the Sea*, edited by P. D. Falkowski and A. D. Woodhead, pp. 89–106, Plenum, New York.

Behrenfeld, M. J., and P. G. Falkowski (1997), A consumers guide to phytoplankton primary production models, *Limnol. Oceanogr.*, *42*(7), 1479–1491.

Bishop, J. K. B., and W. B. Rossow (1991), Spatial and temporal variability of global surface solar irradiance, *J. Geophys. Res.*, *96*(C9), 16,839–16,858.

Bishop, J. K. B., W. B. Rossow, and E. G. Dutton (1997), Surface solar irradiance from ISCCP 1983–1991, *J. Geophys. Res.*, *102*(D6), 6883–6910.

Bopp, L., P. Monfray, O. Aumont, J.-L. Dufresne, H. Le Treut, G. Madec, L. Terray, and J.C. Orr (2001), Potential impact of climate change on marine export production, *Global Biogeochem. Cycles*, *15*(1), 81–100.

Boville, B. A., J. T. Kiehl, P. J. Rasch, and F. O. Bryan (2001), Improvements to the NCAR CSM-1 for transient climate simulations, *J. Clim.*, *14*, 164–179.

Boyd, P. W. (2002), The role of iron in the biogeochemistry of the Southern Ocean and equatorial Pacific: A comparison of in situ iron enrichments, *Deep Sea Res., Part II*, *49*, 1803–1821.

Boyd, P. W., and S. C. Doney (2002), Modeling regional responses by marine pelagic ecosystems to global climate change, *Geophys. Res. Lett.*, *29(16), 1806*, doi:10.1029/2001GL014130.

Boyd, P., J. LaRoche, M. Gall, R. Frew, and R. M. L. McKay (1999), Role of iron, light, and silicate in controlling algal biomass in subantarctic waters southeast of New Zealand, *J. Geophys. Res.*, *104*(C6), 13,395–13,408.

Boyd, P. W., et al. (2000), A mesoscale phytoplankton bloom in the polar Southern Ocean stimulated by iron fertilization, *Nature*, *407*, 695–702.

Bryan, K., and M. J. Spelman (1985), The ocean's response to a CO_2-induced warming, *J. Geophys. Res.*, *90*(C6), 11,679–11,688.

Campbell, J. C. (1995), The lognormal distribution as a model for bio-optical variability in the sea, *J. Geophys. Res.*, *100*(C7), 13,237–13,254.

Campbell, J., et al. (2002), Comparison of algorithms for estimating ocean primary production from surface chlorophyll, temperature, and irradiance, *Global Biogeochem. Cycles*, *16*(3), 1035, doi:10.1029/2001GB001444.

Carr, M.-E. (2002), Estimation of potential productivity in Eastern Boundary Currents using remote sensing, *Deep Sea Res., Part II*, *49*, 59–80.

Christian, J. R., M. A. Verschell, R. Murtugudde, A. J. Busalacchi, and C. R. McClain (2002a), Biogeochemical modelling of the tropical Pacific Ocean: I. Seasonal and interannual variability, *Deep Sea Res., Part II*, *49*, 509–543.

Christian, J. R., M. A. Verschell, R. Murtugudde, A. J. Busalacchi, and C. R. McClain (2002b), Biogeochemical modelling of the tropical Pacific Ocean: II. Iron biogeochemistry, *Deep Sea Res., Part II*, *49*, 545–565.

Corti, S., F. Molteni, and T. M. Palmer (1999), Signature of recent climate change in frequencies of natural atmospheric circulation regimes, *Nature*, *398*, 799–802.

Cox, P. M., R. A. Betts, C. D. Jones, S. A. Spall, and I. J. Totterdell (2000), Acceleration of global warming due to carbon cycle feedbacks in a 3D coupled model, *Nature*, *408*, 184–187.

Cubasch, U., G. A. Meehl, G. J. Boer, R. J. Stouffer, M. Dix, A. Noda, C. A. Senior, S. Raper, and K. S. Yap (2001), Projections of future climate change, in *Climate Change 2001: The Scientific Basis*, edited by J. T. Houghton et al., pp. 525–582, Cambridge Univ. Press, New York.

Dai, A., T. M. L. Wigley, B. A. Boville, J. T. Kiehl, and L. E. Buja (2001), Climates of the twentieth and twenty-first centuries simulated by the NCAR climate system model, *J. Clim.*, *14*, 485–519.

de Baar, H. J. W., J. T. M. de Jong, D. C. E. Bakker, B. M. Löscher, C. Veth, U. Bathmann, and V. Smetacek (1995), Importance of iron for plankton blooms and carbon dioxide drawdown in the Southern Ocean, *Nature*, *373*, 412–415.

de Baar, H. H. W., J. T. N. de Jong, R. F. Nolting, K. R. Timmermans, M. A. van Leeuwe, U. Bathmann, M. R. van der Loeff, and J. Sildam (1999), Low dissolved Fe and the absence of diatom blooms in remote Pacific waters of the Southern Ocean, *Mar. Chem.*, *66*, 1–34.

Denman, K., E. Hofmann, and H. Marchant (1996), Marine biotic responses to environmental change and feedbacks to climate, in *Climate Change 1995*, edited by J. T. Houghton et al., pp. 483–516, Cambridge Univ. Press, New York.

Dixon, K. W., L. Delworth, T. R. Knutson, M. J. Spelman, and R. J. Stouffer (2003), A comparison of climate change simulations produced by two GFDL coupled climate models, *Global Planet. Change*, *37*(1–2), 81–102.

Dufresne, J. L., P. Friedlingstein, M. Berthelot, L. Bopp, P. Ciais, L. Fairhead, H. L. Treut, and P. Monfray (2002), On the magnitude of positive feedback between future climate change and the carbon cycle, *Geophys. Res. Lett.*, *29*(10), 1405, doi:10.1029/2001GL013777.

Fasham, M. J. R., H. W. Ducklow, and S. M. McKelvie (1990), A nitrogen-based model of plankton dynamics in the oceanic mixed layer, *J. Mar. Res.*, *48*(3), 591–639.

Fasham, M. J. R., J. L. Sarmiento, R. D. Slater, H. W. Ducklow, and R. Williams (1993), A seasonal three-dimensional ecosystem model of nitrogen cycling in the North Atlantic euphotic zone: A comparison of the model results with observation from Bermuda Station "S" and OWS "India," *Global Biogeochem Cycles*, *7*(2), 379–415.

Friedlingstein, P., L. Bopp, P. Ciais, J.-L. Dufresne, L. Fairhead, H. LeTreut, P. Monfray, and J. Orr (2001), Positive feedback between future climate change and the carbon cycle on, *Geophys. Res. Lett.*, *28*(8), 1543–1546.

Gargett, A. E. (1998), Physics to fish: Interactions between physics and biology on a variety of scales, *Oceanography*, *10*(3), 128–131.

Gent, P., and J. C. McWilliams (1990), Isopycnal mixing in ocean circulation models, *J. Phys. Oceanogr.*, *20*, 150–155.

Helbling, E. W., V. Villafañe, and O. Holm-Hansen (1991), Effect of iron on productivity and size distribution of Antarctic phytoplankton, *Limnol. Oceanogr.*, *36*(8), 1879–1885.

Hellerman, S., and M. Rosenstein (1983), Normal monthly wind stress over the world ocean with error estimates, *J. Phys. Oceanogr.*, *13*, 1093–1104.

Hirst, A. C., S. P. O'Farrell, and H. B. Gordon (2000), Comparison of a coupled ocean-atmosphere model with and without oceanic eddy-induced advection: I. Ocean spin-up and control integrations, *J. Clim.*, *13*, 139–163.

Hiscock, M. R., J. Marra, W. O. Smith, R. Goericke, C. Measures, S. Vink, R. J. Olson, H. M. Sosik, and R. T. Barber (2003), Primary productivity and its regulation in the Pacific Sector of the Southern Ocean, *Deep Sea Res., Part II*, *50*, 533–558.

Johns, T. C., et al. (2003), Anthropogenic climate change for 1860 to 2100 simulated with the HadCM3 model under updated emissions scenarios, *Clim. Dyn.*, *20*, 583–612.

Laws, E. A., P. G. Falkowski, W. O. Smith Jr., H. Ducklow, and J. J. McCarthy (2000), Temperature effects on export production in the open ocean, *Global Biogeochem. Cycles*, *14*(4), 1231–1246.

Lee, Z. P., K. L. Carder, J. Marra, R. G. Steward, and M. J. Perry (1996), Estimating primary production at depth from remote sensing, *Appl. Opt.*, *35*, 463–474.

Leggett, J., W. J. Pepper, and R. J. Swart (1992), Emissions scenarios for IPCC: An update, in *Climate Change 1992: The Supplementary Report to the IPCC Scientific Assessment*, edited by J. T. Houghton et al., pp. 69–95, Cambridge Univ. Press, New York.

Levitus, S., R. Burgett, and T. Boyer (1994a), *World Ocean Atlas 1994*, vol. 3, *Salinity*, *NOAA Atlas NESDIS 3*, 99 pp., Natl. Oceanic and Atmos. Admin., Silver Spring, Md.

Levitus, S., R. Burgett, and T. Boyer (1994b), *World Ocean Atlas 1994*, vol. 4, *Temperature*, 117 pp., Natl. Oceanic and Atmos. Admin., Silver Spring, Md.

Levitus, S., T. P. Boyer, M. E. Conkright, T. O'Brien, J. Antonov, C. Stephens, L. Stathoplos, D. Johnson, and R. Gelfeld (1998), *World Ocean Database 1998*, vol. 1, *Introduction*, *NOAA Atlas NESDIS 18*, 346 pp., Natl. Oceanic and Atmos. Admin., Silver Spring, Md.

Longhurst, A. (1994), *Ecological Geography of the Ocean*, 176 pp., Academic, San Diego, Calif.

Maier-Reimer, E. (1993), Geochemical cycles in an ocean general circulation model: Preindustrial tracer distributions, *Global Biogeochem. Cycles*, *7*(3), 645–677.

Manabe, S., and R. J. Stouffer (1996), Low-frequency variability of surface air temperature in a 1000-year integration of a coupled atmosphere-ocean-land surface model, *J. Clim.*, *9*, 376–393.

Manabe, S., R. J. Stouffer, M. J. Spelman, and K. Bryan (1991), Transient responses of a coupled ocean-atmosphere model to gradual changes of atmospheric CO_2: 1. Annual mean response, *J. Clim.*, *4*, 785–818.

Marra, J., C. Ho, and C. C. Trees (2003), An algorithm for the calculation of primary productivity from remote sensing data, 27 pp., Lamont-Doherty Earth Obs., Palisades, N. Y.

Martin, J. H., R. M. Gordon, and S. E. Fitzwater (1991), The case for iron, *Limnol. Oceanogr.*, *36*, 1793–1802.

Matear, R. J., A. C. Hirst, and B. I. McNeil (2000), Changes in dissolved oxygen in the Southern Ocean with climate change, *Geochem. Geophys. Geosyst.*, *1*, Paper number 20000GC000086.

McAvaney, B. J., C. Covey, S. Joussaume, V. Kattsov, A. Kitoh, W. Ogana, A. J. Pitman, A. J. Weaver, R. A. Wood, and Z.-C. Zhao (2001), Model evaluation, in *Climate Change 2001: The Scientific Basis*, edited by J. T. Houghton et al., pp. 471–524, Cambridge Univ. Press, New York.

Moore, K. J., S. C. Doney, J. A. Kleypas, D. M. Glover, and I. Y. Fung (2002), An intermediate complexity marine ecosystem model for the global domain, *Deep Sea Res., Part II*, *49*, 463–507.

Nakicenovic, N., et al. (2000), *IPCC Special Report on Emissions Scenarios*, 599 pp., Cambridge Univ. Press, New York.

Oberhuber, J. M. (1993), Simulation of the Atlantic circulation with a coupled sea ice-mixed layer- isopycnal general circulation model: I. Model description, *J. Phys. Oceanogr.*, *23*, 808–829.

Platt, T., and S. Sathyendranath (1988), Oceanic primary production: Estimation by remote sensing at local and regional scales, *Science*, *241*, 1613–1620.

Platt, T., and S. Sathyendranath (1999), Spatial structure of pelagic ecosystem processes in the global ocean, *Ecosystems*, *2*, 384–394.

Potter, C. S., J. T. Randerson, C. B. Field, P. A. Matson, P. M. Vitousek, H. A. Mooney, and S. A. Klooster (1993), Terrestrial ecosystem production: A process model based on global satellite and surface data, *Global Biogeochem. Cycles*, *7*(4), 811–841.

Raper, S. C. B., J. M. Gregory, and R. J. Stouffer (2002), The role of climate sensitivity and ocean uptake on AOGCM transient temperature response, *J. Clim.*, *15*, 124–130.

Reid, J., E. Brinton, A. Fleminger, E. L. Venrick, and J. A. McGowan (1978), Ocean circulation and marine life, in *Advances in Oceanography*, edited by H. Charnock and G. Deacon, pp. 65–130, Plenum, New York.

Roeckner, E., L. Bengtsson, J. Feichter, J. Lelieveld, and H. Rodhe (1999), Transient climate change simulations with a coupled atmosphere-ocean GCM including the tropospheric sulfur cycle, *J. Clim.*, *12*, 3004–3032.

Sarmiento, J. L., R. D. Slater, M. J. R. Fasham, H. W. Ducklow, J. R. Toggweiler, and G. T. Evans (1993), A seasonal three-dimensional ecosystem model of nitrogen cycling in the North Atlantic euphotic zone., *Global Biogeochem. Cycles*, *7*(2), 417–450.

Schimel, D., et al. (2000), Contribution of increasing CO_2 and climate to carbon storage by ecosystems in the United States, *Science*, *287*, 2004–2006.

Smith, W. O., Jr., R. T. Barber, M. R. Hiscock, and J. Marra (2000), The seasonal cycle of phytoplankton biomass and primary productivity in the Ross Sea, Antarctica, *Deep Sea Res., Part II*, *47*, 3119–3140.

Sprintall, J., and M. Tomczak (1992), Evidence of the barrier layer in the surface-layer of the tropics, *J. Geophys. Res.*, *97*(C5), 7305–7316.

Stone, D. A., A. J. Weaver, and R. J. Stouffer (2001), Projections of climate change onto modes of atmospheric variability, *J. Clim.*, *14*, 3551–3565.

Sverdrup, H. U. (1955), The place of physical oceanography in oceanographic research, *J. Mar. Res.*, *14*(4), 287–294.

R. S. Barber, Duke University, 135 Duke Marine Lab Road, Beaufort, NC 28516, USA.

L. Bopp and P. Monfray, Laboratoire des Sciences du Climat et de l'Environnement, Unite Mixte de Recherche CEA-CNRS, LSCE, CEA Saclay, Bat. 709 - Orme, F-91191 Gif-sur-Yvette, France.

S. C. Doney, Department of Marine Chemistry and Geochemistry, Woods Hole Oceanographic Institution, 360 Woods Hole Rd., Woods Hole, MA 02543, USA.

A. C. Hirst, CSIRO Atmospheric Research, PMB 1, Aspendale, Victoria 3195, Australia.

J. Kleypas, Climate and Global Dynamics, National Center for Atmospheric Research, P.O. Box 3000, Boulder, CO 80307, USA.

R. Matear, CSIRO Division of Marine Research, GPO Box 1538, Hobart, Tasmania 7001, Australia.

U. Mikolajewicz, Max-Planck-Institut für Meteorologie, Bundsstrasse 55, D-20146 Hamburg, Germany.

J. L. Sarmiento and R. Slater, Atmospheric and Oceanic Sciences Program, Princeton University, PO Box CN710, Princeton, NJ 08544, USA. (jls@princeton.edu)

V. Soldatov, Institute of Physics, St. Petersburg State University, Ul'yanovskaya 1, St. Petersburg, 198904, Russia.

S. A. Spall, Met Office, Hadley Centre for Climate Prediction and Research, London Road, Bracknell, Berkshire RG12 2SY, UK.

R. Stouffer, Geophysical Fluid Dynamics Laboratory, Princeton, NJ 08542, USA.

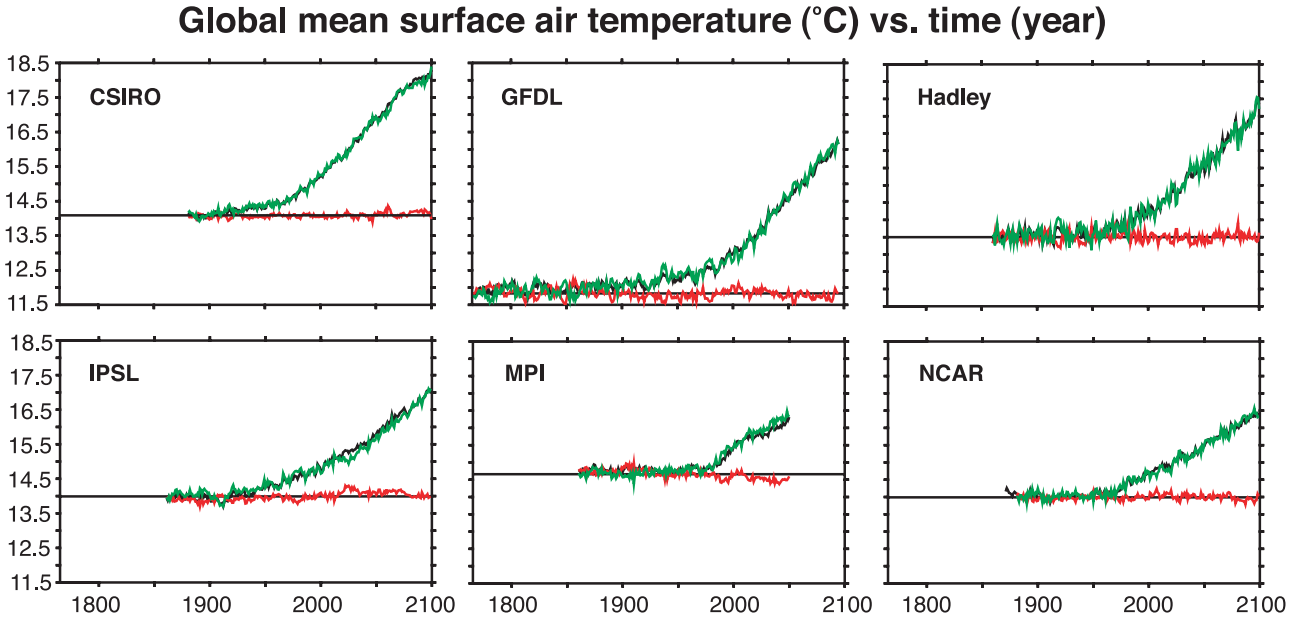

Figure 1. Time-dependent plots of mean surface air temperature for all six coupled climate models. The red line is the control scenario, the green line is the climate warming scenario, and the black line is the climate warming scenario minus the control scenario.

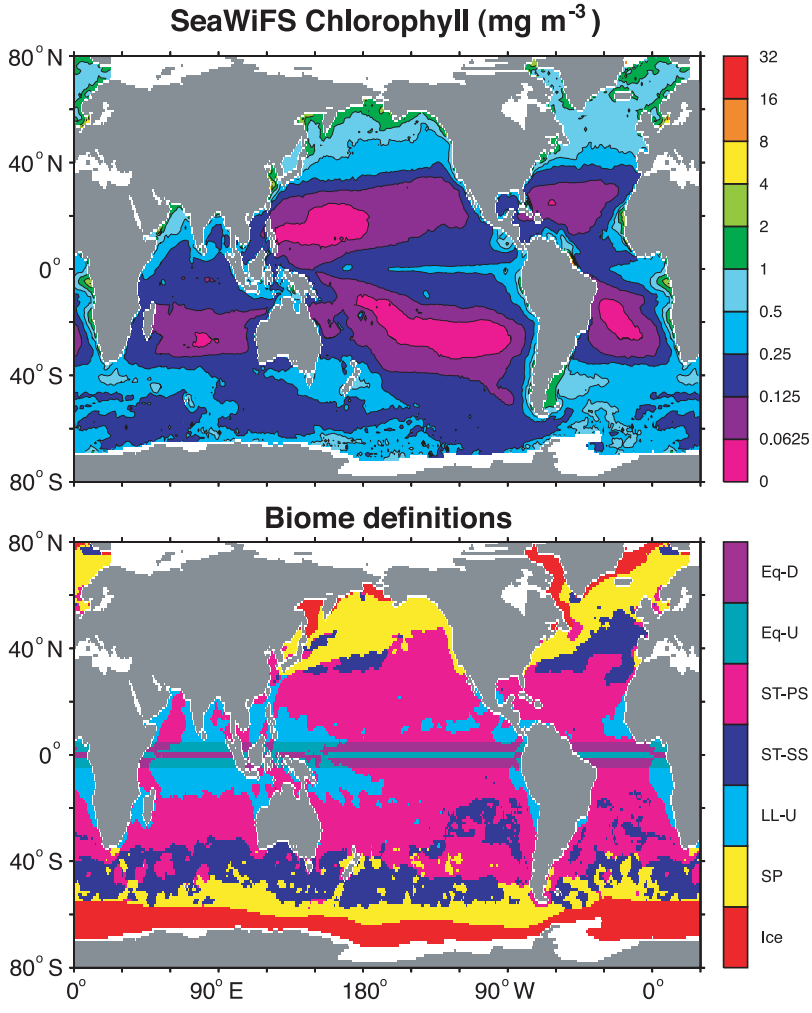

Figure 2. (a) Annual mean SeaWiFS chlorophyll from Yoder and Kennelly (online data set, 2001). (b) Biome classification scheme calculated using mixed layer depths obtained from observed density and from upwelling calculated from the wind stress divergence using observed winds. The equatorially influenced biome covers the area between 5°S and 5°N, and is colored a dirty light blue in areas where upwelling occurs (labeled "Eq-U" on the color bar) and dark pink in areas where downwelling occurs (labeled "Eq-D"). Outside of this band, the region labeled "Ice" (red) is the marginal sea ice biome, the region labeled "SP" (yellow) is the subpolar biome, the region labeled "LL-U" (light blue) is the low-latitude upwelling biome, the region labeled "ST-SS" (dark blue) is the seasonally mixed subtropical gyre biome, and the region labeled "ST-PS" (pink) is the permanently stratified subtropical gyre biome.

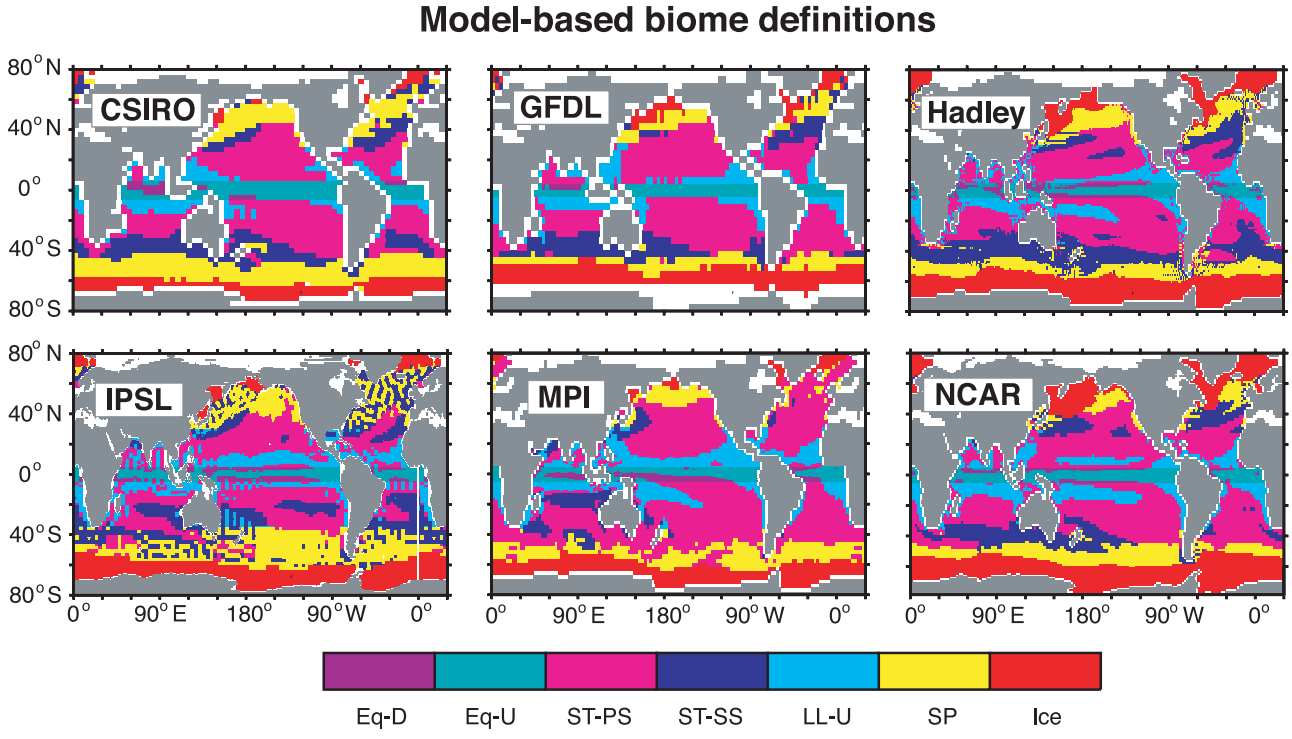

Figure 3. Biome classifications as determined from the AOGCM control climate variables for each of the six models. The color scheme and symbols are described in the Figure 2 caption.

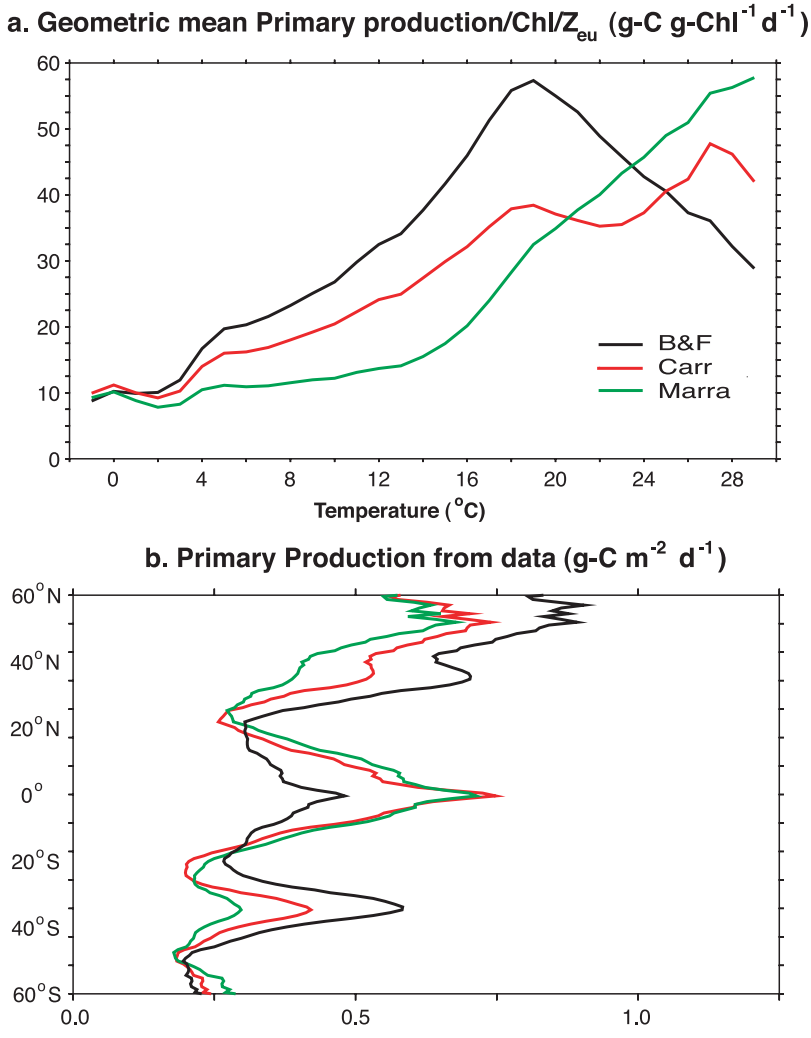

Figure 4. Primary production derived from SeaWiFS chlorophyll and observed light and temperature using the *Behrenfeld and Falkowski* [1997], *Carr* [2002], and *Marra et al.* [2003] algorithms (B&F, Carr, and Marra, respectively). (a) Primary production normalized by chlorophyll and euphotic zone depth (Z_{eu}) and then binned and averaged in 1°C bins. Z_{eu} is derived from the implied vertical distribution of chlorophyll as part of the three primary production algorithms. (b) Zonal mean primary production.

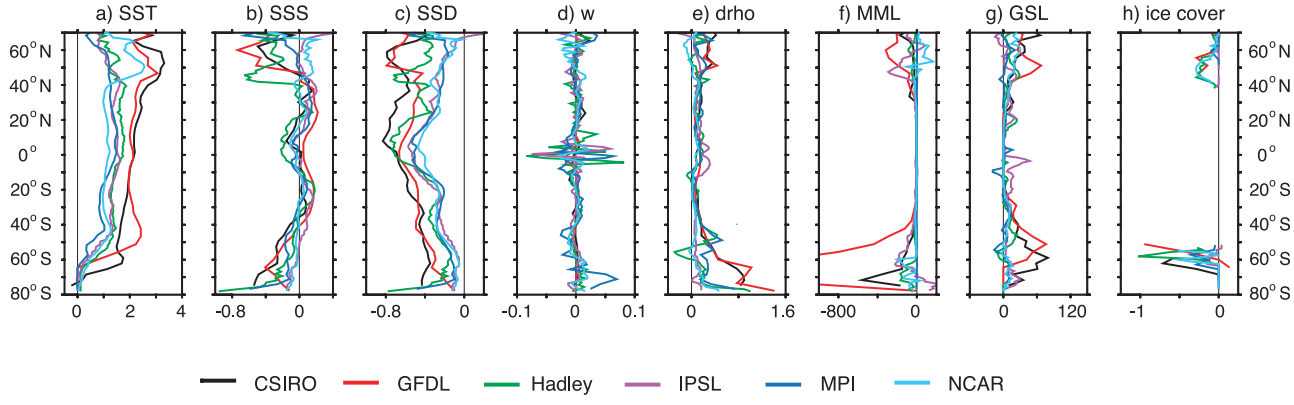

Figure 5. Zonal mean response to climate change (warming minus control) averaged over the period 2040 to 2060 (except for MPI, which is for the period 2040 to 2049) of (a) sea surface temperature, SST in °C, (b) sea surface salinity, SSS in practical salinity units (PSU), (c) sea surface potential density, SSD ($\sigma_\theta \equiv \rho - 1000$ kg m^{-3}), (d) upwelling velocity, w, in m d^{-1}, (e) the fractional change in the vertical density gradient, drho, (f) the wintertime maximum mixed layer depth, MML, in m, (g) the growing season length, GSL, in days, and (h) the ocean area of maximum wintertime sea ice extent in 10^{12} m^2 per degree.

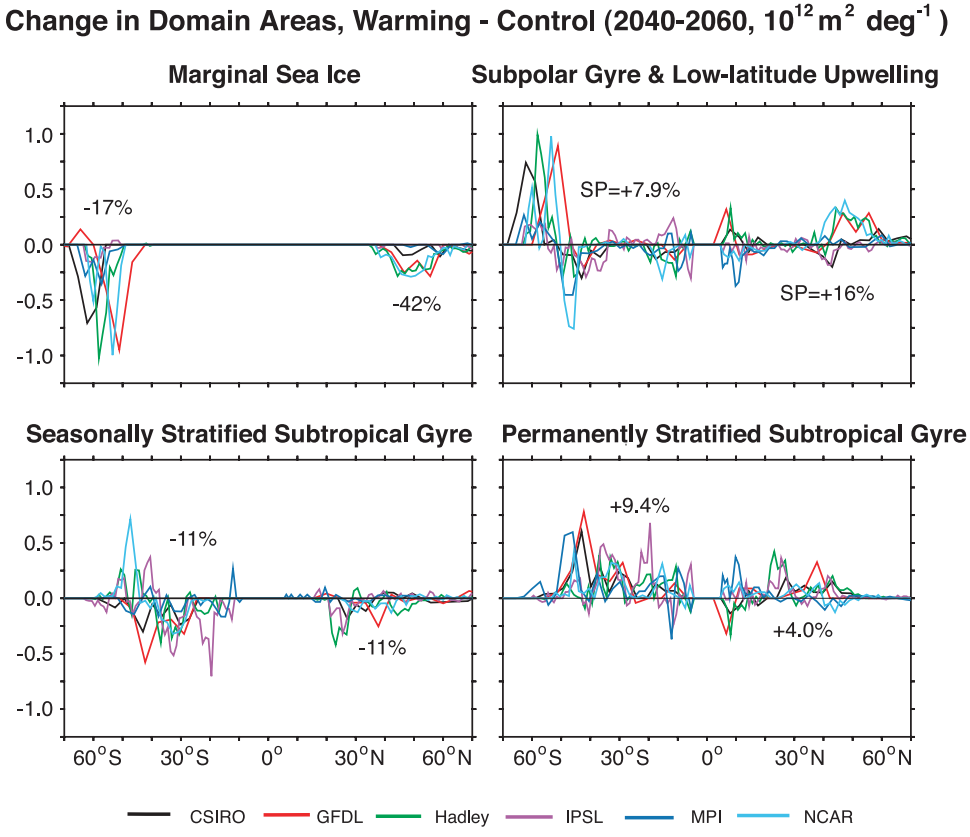

Figure 6. Zonally integrated changes in biome areas (warming minus control) for the six models. The units are 10^{12} m^2 per degree. Percent changes are also shown. The percent change for the combined subpolar gyre and low latitude upwelling biomes is just that due to the contribution of the subpolar gyre biome (SP).

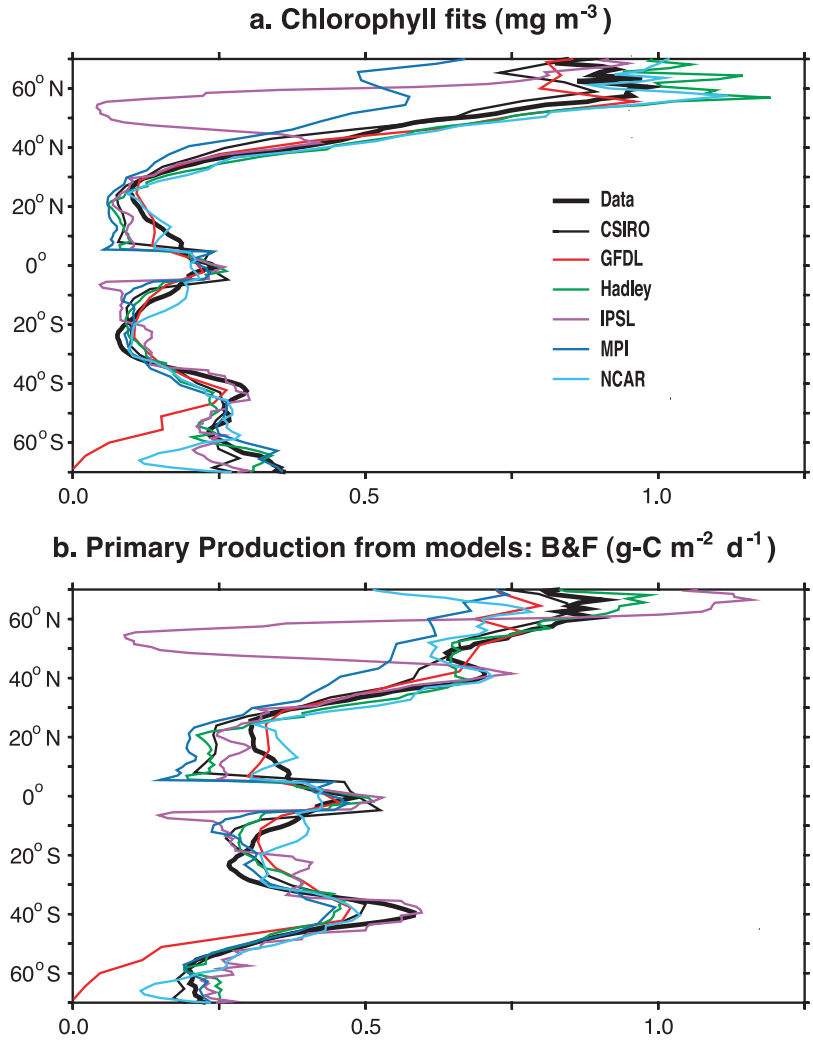

Figure 7. Zonal means of chlorophyll and primary production. (a) Chlorophyll in mg m^{-3} estimated using SeaWiFS color observations (thick black line) and chlorophyll estimated from AOGCM variables using the empirical model described in the text (thin lines). The model labels correspond to those given in Table 1. (b) Primary production in g m^{-2} d^{-1} of carbon derived from the SeaWiFS chlorophyll using the *Behrenfeld and Falkowski* [1997] algorithm. The line colors correspond to those in Figure 7a.

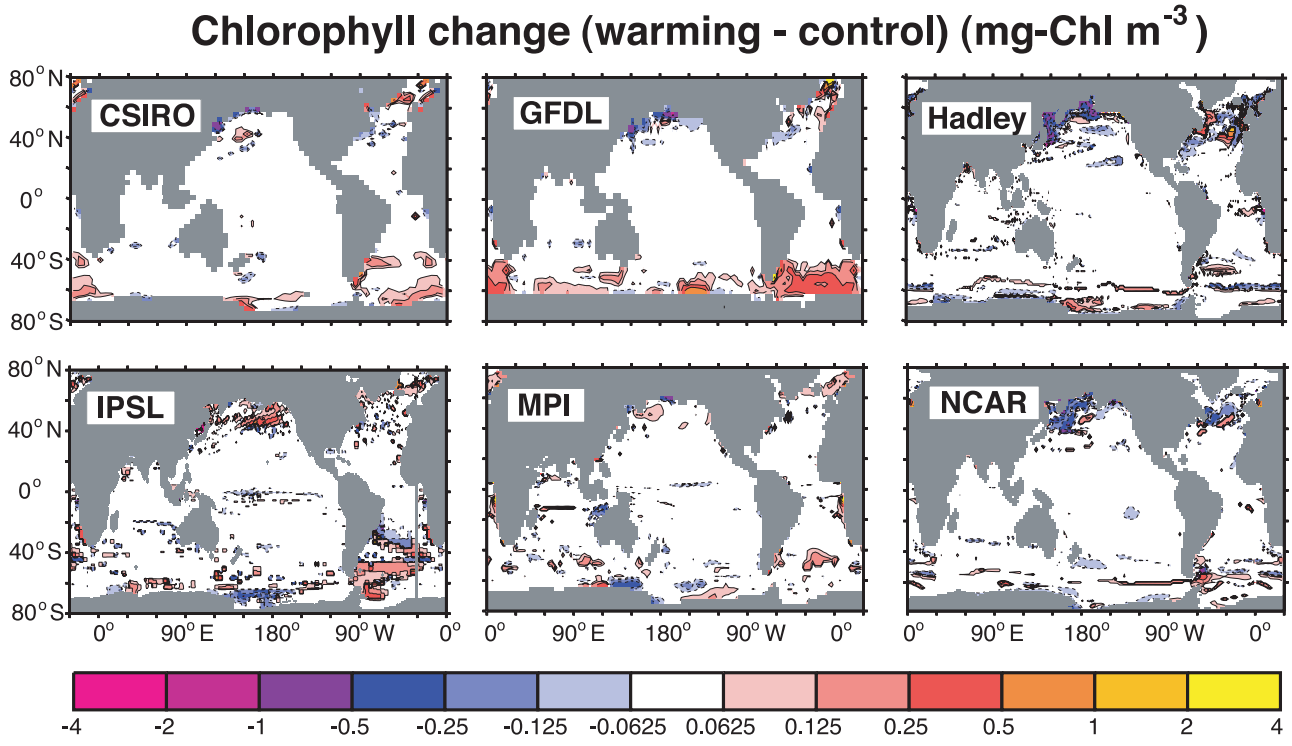

Figure 8. Impact of the global warming simulations on the chlorophyll concentration in mg m^{-3}. Chlorophyll is calculated for both the control and the warming simulations using the empirical model (equation (2)). The figure shows the difference between the warming simulation and the control simulation averaged over the period 2040 to 2060 (except for MPI, which is for the period 2040 to 2049). Areas in white are those for which the chlorophyll change is smaller than ±0.0625 mg m^{-3}.

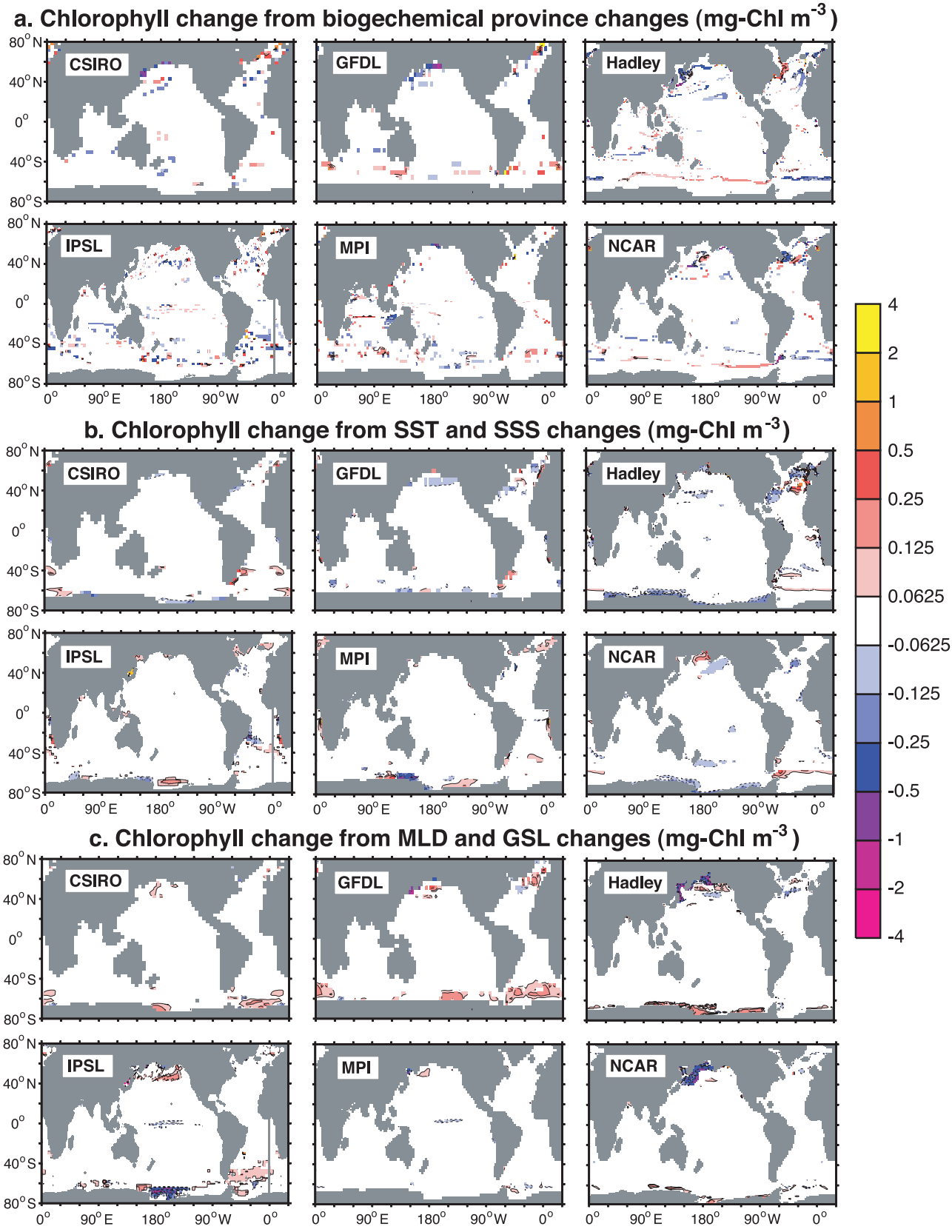
a. Chlorophyll change from biogechemical province changes (mg-Chl m-3)
b. Chlorophyll change from SST and SSS changes (mg-Chl m-3)
c. Chlorophyll change from MLD and GSL changes (mg-Chl m-3)
CSIRO
GFDL
Hadley
IPSL
MPI
NCAR
80°N
40°N
0°
40°S
80°S
0°
90°E
180°
90°W
4
2
1
0.5
0.25
0.125
0.0625
-0.0625
-0.125
-0.25
-0.5
-1
-2
-4

Figure 9

Figure 9. Impact of the global warming simulations on the chlorophyll concentration in mg m^{-3} as in Figure 8, but broken down into various components. The global ocean is first separated into regions where the biogeographical provinces changed from one to another (e.g., marginal ice biome to subpolar biome) and regions where it did not. (a) Contribution to the total chlorophyll response that occurs in regions where the biogeographical provinces changed. (b, c) Changes in regions where the biogeographical provinces remained the same. Figure 9b shows the contribution to the total chlorophyll response that is due to changes in water mass properties: sea surface temperature anomaly (SST') and sea surface salinity anomaly (SSS') calculated using equation (4). Figure 9c shows the contribution to the total chlorophyll response that is due to the combined influence of changes in the maximum wintertime mixed layer depth (MLD) and the growing season length (GSL), again calculated using equation (4). The sum of Figures 9a, 9b, and 9c is approximately but not exactly equal to Figure 8 because of the nonlinearity of the chlorophyll empirical equation, which means that the breakdown given by equation (4) is not exact.

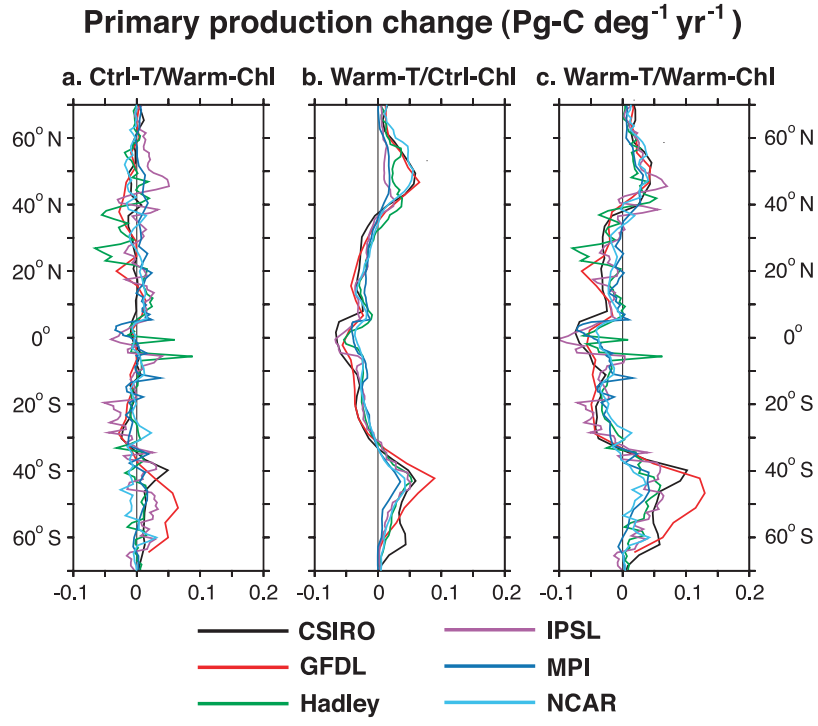

Figure 10. Zonally integrated response of primary production calculated with the *Behrenfeld and Falkowski* [1997] algorithm using chlorophyll calculated from the empirical model (equation (2)). The figure shows the difference between the warming and the control simulation for each of the six AOGCMs averaged over the period 2040 to 2060 (except for MPI, which is for the period 2040 to 2049). (a) The increase in primary production that occurs in response to the chlorophyll change only, with temperature kept constant at the control scenario. (b) The increase in primary production that occurs in response to the temperature increase only, with chlorophyll kept constant at the control scenario. (c) The increase in primary production that occurs in response to the combined effect of the chlorophyll change and temperature increase.

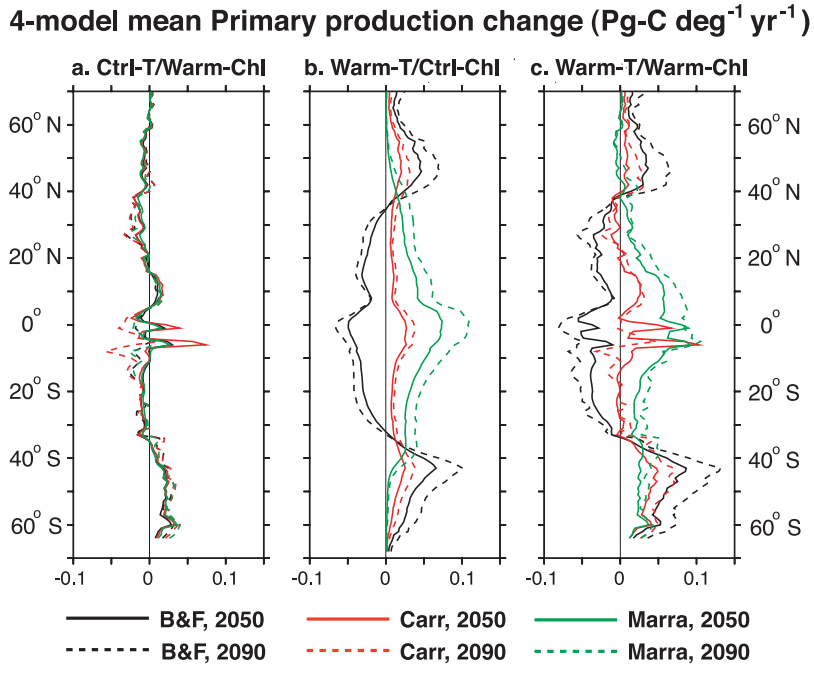

Figure 11. The mean over the CSIRO, GFDL, Hadley, and NCAR models of the response of zonally integrated primary production to global warming. The MPI and IPSL models are excluded, the former because the simulation ended in 2049, the latter because of the difficulties encountered in defining the biome boundaries; compare Figure 3. The primary production responses are calculated as in Figure 10 (warming minus control), but with the three different primary production algorithms of *Behrenfeld and Falkowski* [1997] (B&F), *Carr* [2002] (Carr), and *Marra et al.* [2003] (Marra). The figure shows both the average over the period 2040 to 2060 (labeled 2050) and the average over the period 2080 to 2100 (labeled 2090). The three panels are calculated as described in the Figure 10 caption.